

Kinetics of ‘blue’ flames in the gas-phase oxidation and combustion of hydrocarbons and their derivatives

V Ya Basevich, S M Frolov

Contents

I. Introduction	867
II. Cool and blue flames	867
III. Modelling of gas-phase oxidation of acetaldehyde and hydrocarbons C ₁ –C ₇	870
IV. Conclusion	883

Abstract. Experimental and calculated data on the kinetics of ‘blue’ flame observed in the gas-phase oxidation and combustion of hydrocarbons and their derivatives are considered. It is shown that blue flames arise due to the decomposition of hydrogen peroxide that forms in the oxidation of hydrocarbons. They manifest themselves by light emission, are identified by partial heat release (the appearance of a step in the time dependences of temperature and pressure observed in closed-vessel experiments) and propagate as conventional hot flames. The bibliography includes 43 references.

I. Introduction

Oxidation and combustion of hydrocarbons play an important role in chemical engineering, power production in thermal machines of various types and in environmental control. Being started quite long ago, their studies achieved considerable progress only in the second half of the 20th century. By that time, it was reliably stated that slow gas-phase oxidation of hydrocarbons represents a radical-chain reaction with degenerate branches. Kinetic studies of low-temperature oxidation of hydrocarbons have demonstrated its multistage nature. It is assumed that low-temperature oxidation and combustion of hydrocarbons involves the stages of cool, blue and hot flames. All these stages were observed experimentally. Thus cool flames were observed back in 1882 for the hydrocarbon oxidation in heated vessels.¹ Further studies of low-temperature oxidation of hydrocarbons demonstrated that this process represents partial oxidation to afford valuable oxygen-containing products such as alcohols, aldehydes, acids and peroxides. This explains the keen attention drawn to the cool-flame oxidation of hydrocarbons (*e.g.*, see monographs^{2–4} and references therein). However, whereas to date the mechanism of the appearance of cool flame can be considered as understood with a large degree of confidence, the mechanism of the emergence of blue flames is still largely unknown.

V Ya Basevich, S M Frolov N N Semenov Institute of Chemical Physics, Russian Academy of Sciences, ul. Kosygina 4, 119991 Moscow, Russian Federation. Fax (7-495) 137 61 30, tel. (7-495) 939 74 52, e-mail: basevich@center.chph.ras.ru (V Ya Basevich), tel. (7-495) 939 72 28, e-mail: smfrol@center.chph.ras.ru (S M Frolov)

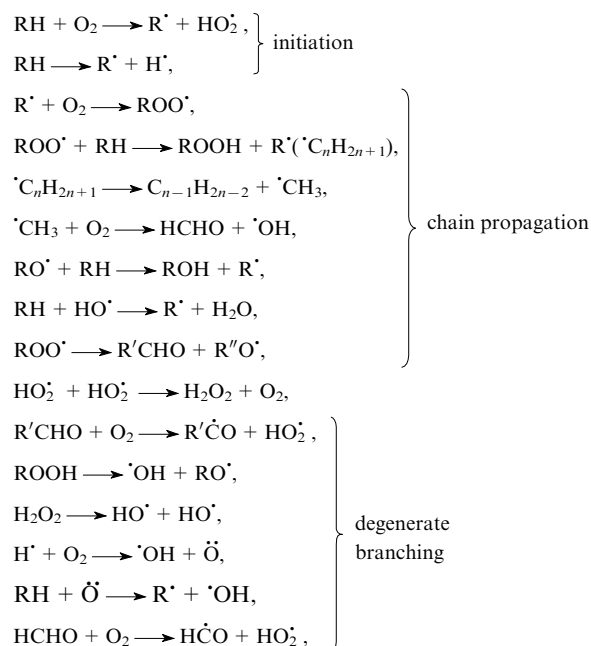
Received 7 March 2007

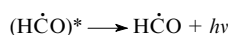
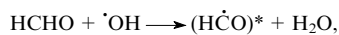
Uspekhi Khimii 76 (9) 927–944 (2007); translated by T Ya Safonova

Blue flames manifest themselves by light emission and can be identified by a partial heat release (the appearance of a step in curves that describe the time dependences of pressure and temperature in closed-vessel experiments). They can propagate like conventional hot flames. Blue flames were observed in the gas-phase oxidation and combustion of methane, ethane, n-heptane, isooctane and benzene as well as of acetaldehyde and diethyl ether. Experimental and theoretical studies of blue flames observed in the low-temperature oxidation of hydrocarbons and their derivatives are closely associated with the studies of cool flames; hence, the latter will also be briefly considered in this review, especially as both cool and blue flames pertain to low-temperature flames and their separation is a difficult task.

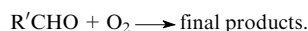
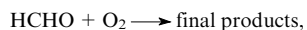
II. Cool and blue flames

It is well known that low-temperature oxidation of hydrocarbons follows the radical-chain mechanism with degenerate branching, where the branching is due to either the decomposition of hydroperoxides formed in the reaction or the interaction of aldehydes formed with oxygen. The main steps of this reaction are as follows:





and *etc.*,



The appearance of cool flame in hydrocarbon oxidation is due to the glow of excited formaldehyde. Blue flame arises as a result of further conversion of hydrocarbons owing to the glow of both excited formaldehyde and formyl radicals. Cool flames are observed at both low and high pressures typical of internal combustion engines (ICE).

The majority of scientists who studied the low-temperature oxidation of hydrocarbons assumed that cool flame arises as a result of explosive decomposition of organic hydroperoxides after their concentration has exceeded a certain critical value (*e.g.*, see Ref. 5). (As a rule, the decomposition is caused by the temperature increase in the course of the reaction). Due to the degenerate branching of the reaction as a result of the hydroperoxide decomposition and also due to the appearance of active species $\cdot\text{OH}$, the process sharply accelerates, heat is released, the temperature and the pressure increase, which leads to the appearance of cool flame.

Figure 1 shows typical kinetic curves of pentane cool-flame oxidation that represent the changes in the overall pressure during the reaction as a result of branching.² Cool flame is identified as a small pressure peak in the $\Delta P(t)$ curve, particularly, at the lowest initial pressure $P_0 = 225$ mm Hg, cool flame appears with a delay $t_i = 120$ s. As the initial pressure increases, the cool-flame delay shortens and the intensity (the pressure peak height) increases. Ultimately, at a pressure $P_0 = 340$ mm Hg, the cool-flame step is followed by hot autoignition, which is accompanied by a strong increase in the pressure (marked by an arrow). This is the so-called two-stage autoignition.

If the cool flame has failed to be transformed into the hot flame so that the reaction mixture is cooled from the vessel walls and also if the initial concentrations of fuel and oxidant have changed insignificantly in the cool flame, the autoignition can be repeated. This is the mechanism of origination of multiple (periodic) cool flames.

Figure 2 shows kinetic curves of cool-flame oxidation of ethyl methyl ketone.⁶ As is seen, cool flames appear twice during the oxidation (1 cf and 2 cf). Figure 3 shows a cool flame region confined by the first cool flame region (light circles) on the one side and a region of hot autoignition (dark

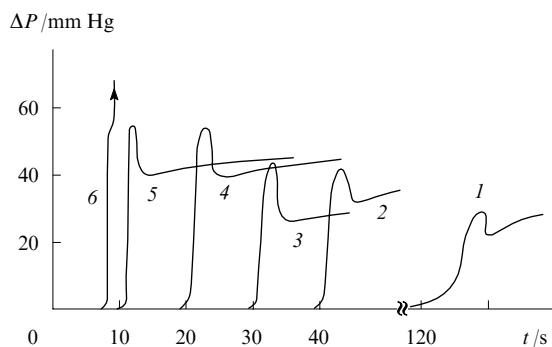


Figure 1. Kinetic curves of cool-flame oxidation of pentane (mixture composition: $n\text{-C}_5\text{H}_{12} + 4\text{O}_2$) for initial temperature $T_0 = 591$ K. Initial pressure $P_0/\text{mm Hg}$: (1) 225, (2) 250, (3) 280, (4) 320, (5) 330, (6) 340.

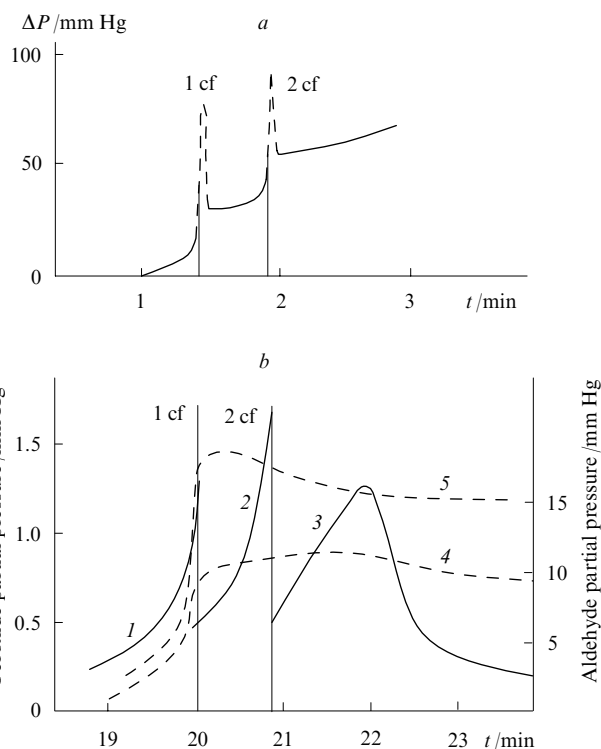


Figure 2. Kinetic curves of cool-flame oxidation of ethyl methyl ketone (mixture composition: $\text{CH}_3\text{COC}_2\text{H}_5 + \text{O}_2$).⁶

(a) Increase in the overall pressure (ΔP); (b) increase in partial pressures of peroxides (curves 1–3), formaldehyde (4) and higher aldehydes (5) in periodic cool flames.

Initial conditions: (a) $P_0 = 32$ kPa, $T_0 = 563$ K (in the presence of acetaldehyde $P_{\text{CH}_3\text{CHO}} = 0.27$ kPa); (b) $P_0 = 40$ kPa, $T_0 = 556$ K.

circles) on the other side in the coordinates 'initial temperature vs. initial pressure'.⁶

As the temperature increases, the formation of peroxides is hindered and, if the concentrations of initial hydrocarbon and oxygen have decreased significantly during the reaction, the oxidation process may be decelerated and even stop but may also continue (depending on conditions) by other reaction channels.

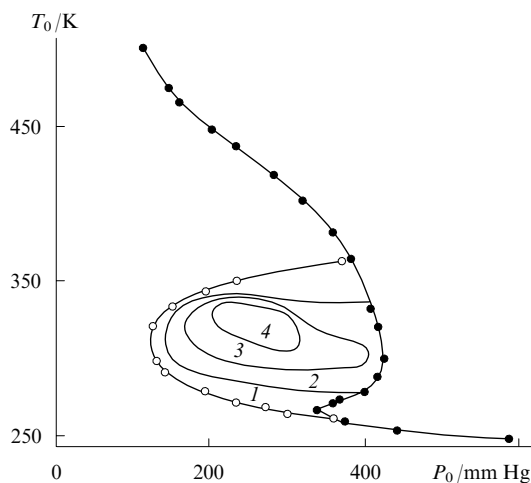


Figure 3. Region of periodic cool flames in equimolar methyl ethyl ketone mixtures with oxygen (numbers within the cool-flame region designate the number of flames).⁶

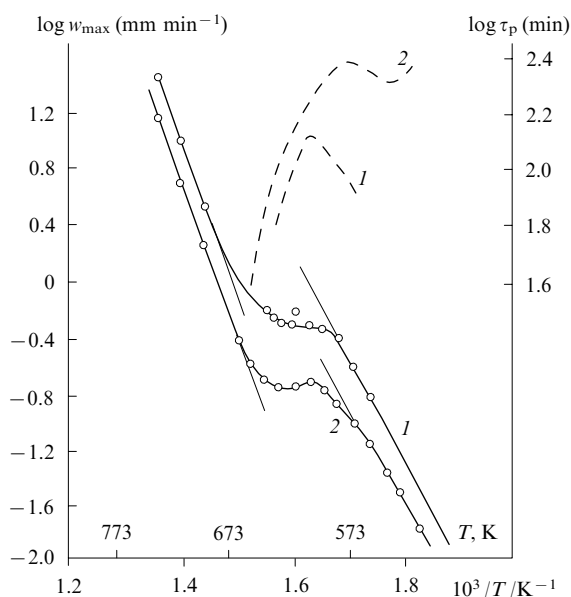


Figure 4. Logarithms of maximum oxidation rate w_{\max} (solid lines) and delay period τ_p (dash lines) for different temperatures.⁷ Mixture $\text{C}_2\text{H}_6 + 0.5\text{O}_2$; (1) $E = 30.0\text{--}33.6 \text{ kcal mol}^{-1}$, $P_0 = 67 \text{ kPa}$; (2) $E = 55.6 \text{ kcal mol}^{-1}$, $P_0 = 83 \text{ kPa}$.

Cold flames are associated with yet another peculiarity of the oxidation kinetics of hydrocarbons and their derivatives, *viz.*, the presence of a region of the negative temperature coefficient (NTC) in which the reaction rate decreases (or remains unchanged) rather than increases with the increase in temperature (Fig. 4).⁷ This phenomenon is associated with the fact that with the increase in temperature in the course of the reaction (or at an elevated initial temperature), the peroxide formation is hindered and the earlier formed peroxides easily decompose. In this case, the reaction branching that involves peroxides ceases to be dominant and the oxidation continues by other channels, which are not so efficient in the NTC region. As a result, in this temperature range, the rate turns out to be

lower at higher temperatures than at lower temperatures. Below, this phenomenon will be considered in more detail.

The first records of blue flames can be found in the studies by Townend *et al.* (*e.g.*, see Ref. 8 and a monograph² and references therein). They studied cool flames that arise at the ignition of fuel–air mixtures with a heated spiral and observed that the cool flame was followed by the appearance of a second brighter flame that propagated through the vessel. They named this phenomenon blue flame. Blue flames were accompanied by a higher (50–250 °C) warming up of the reaction mixture and brighter glow of excited formaldehyde as compared with cool flames.

Blue flames immediately precede the hot autoignition of hydrocarbons. It is assumed that in blue flame hydrocarbons undergo more extensive transformations as compared with cool flame. In addition to the glow of excited formaldehyde, which is inherent in cool flame, the glow at the wavelength of the formyl radical HC^*O is observed. Figure 5 shows experimental data obtained in the studies of autoignition of isooctane–air mixtures in closed vessels.³ In Fig. 5e, three pressure waves are well distinguishable, namely, the first cool-flame wave, the second blue-flame wave and the third wave of the hot explosion. The blue flame period (second wave) corresponds to the delay (induction period) of the hot explosion. In Fig. 5e, this delay is designated as τ_3 .

One piece of evidence for the multistage mechanism of the low-temperature autoignition of hydrocarbons is the appearance of blue flame in the experiments on the autoignition of 'lean' methane–air and isooctane–air mixtures carried out in ICE at temperatures and pressures near the autoignition point. However, no blue flame was observed in the subsequent experiments in a static bomb at the same temperatures and pressures. The later experiments with ICE also demonstrated the appearance of blue flames in the autoignition region of lean methane–air mixtures and benzene mixtures with oxygen. Hence, it seems that the appearance of blue flames during the autoignition processes in fuel–air mixtures in ICE is reliably ascertained (*e.g.*, see Ref. 3 and references therein).

In contrast to multistage high-temperature autoignition of hydrocarbons, the high-temperature autoignition develops continuously without any intermediate stages and ends with hot flame.

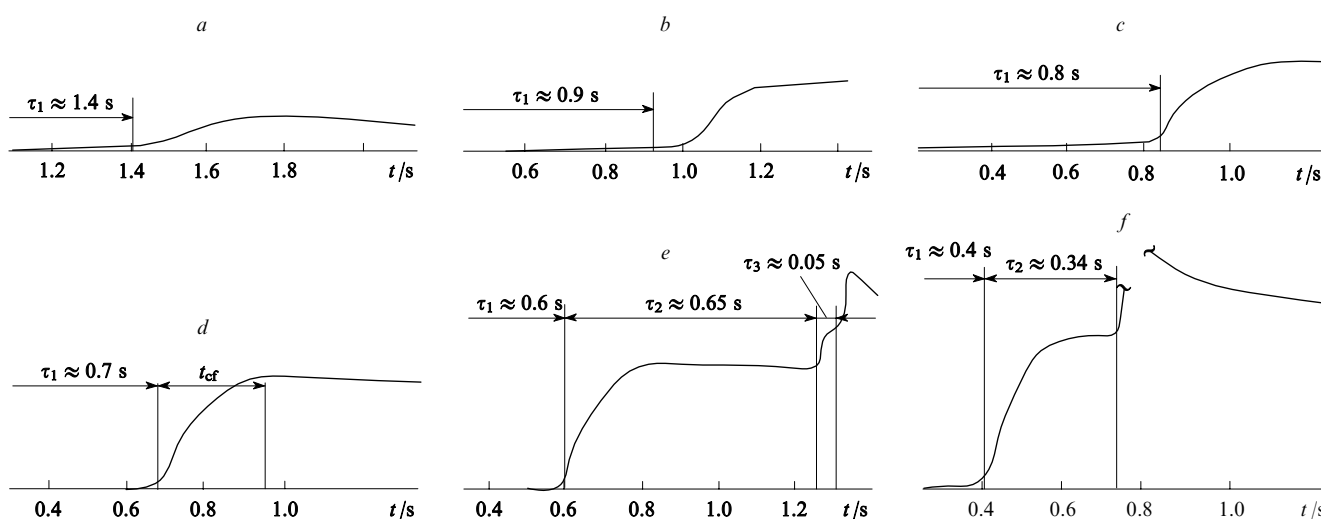


Figure 5. Pressure variation at autoignition of isooctane–air mixtures (stoichiometric ratio $\phi = 1.25$).³ The gain in pressure in the course of the reaction was measured for $T_0 = 643 \text{ K}$ and different initial pressures.

(a) $P_0 = 80 \text{ kPa}$, $P_{\text{ct}}/P_0 = 1.8$; (b) $P_0 = 105 \text{ kPa}$, $P_{\text{ct}}/P_0 = 1.09$; (c) $P_0 = 140 \text{ kPa}$, $P_{\text{ct}}/P_0 = 1.1$; (d) $P_0 = 180 \text{ kPa}$, $P_{\text{ct}}/P_0 = 1.13$; (e) $P_0 = 230 \text{ kPa}$, $P_{\text{ct}}/P_0 \approx 1.14$; (f) $P_0 = 320 \text{ kPa}$, $P_{\text{ct}}/P_0 \approx 1.2$.

Experimental results on the gas-phase oxidation of different hydrocarbons obtained in the mid-20th century are thoroughly described in several monographs.²⁻⁴

III. Modelling of gas-phase oxidation of acetaldehyde and hydrocarbons C₁–C₇

For a long time, a concept on the multistage autoignition mechanism of hydrocarbons was not discussed in the literature. The first publications^{9,10} on the oxidation of hydrocarbons at elevated temperatures and pressures, which merely mentioned cool and blue flames but did not establish any new facts, appeared only in the 1980s.

In the long period during which the hydrocarbon oxidation and combustion were studied, numerous kinetic schemes were proposed that described sufficiently comprehensively the oxidation and combustion of particular hydrocarbons, for instance, radical-chain schemes of oxidation and combustion of methane,^{2,4,11,12} ethane,¹³ propane,¹⁴⁻¹⁶ n-butane,^{17,18} n-pentane,^{19,20} n-heptane,²¹⁻²³ n-octane and isooctane.²⁴ These schemes adequately describe many aspects of hydrocarbon oxidation and combustion, agree with experimental data and allow one to model the corresponding processes. However, if a process can be modelled, then it is sufficiently understood and can be reproduced on the quantitative level. The simultaneous consideration of the known kinetic schemes of oxidation of hydrocarbons and their derivatives allowed the general comprehensive kinetic mechanism of oxidation and combustion of hydrocarbons to be proposed (Table 1 shows such a mechanism for hydrocarbons C₁–C₂; for simplicity, the radical signs in this and the subsequent Table are omitted); however, even incomplete knowledge of all reaction channels and the use of very approximate reaction rate constants often allows one to adequately describe the experimentally observed kinetics of oxidation and combustion using appropriate calculations.

For oxidation of hydrocarbons with ≥ 3 carbon atoms, the cool flames were modelled and the calculations were carried

out that perfectly described the characteristics of these flames.¹⁴⁻²⁴ However, none of these studies considered blue flames and the mechanism of their origination. Papers on the modelling of blue flames were absent in the literature, which stimulation us to dwell into this issue.

As was mentioned above, blue flames are experimentally identified by glow and a stepwise gain in pressure observed in closed-vessel experiments. The detection of the blue-flame glow apparently provides little information on the chemical reactions responsible for its appearance; hence, the data on the variations of pressure and, correspondingly, temperature in the course of oxidation attract keen attention for the identification of blue flames. This information can be retrieved from calculations on the simulation of oxidation and combustion processes, which allows one to determine the temperature, the pressure and the concentrations of all products.

Calculations based on kinetic schemes constructed for the low-temperature oxidation of hydrocarbons involve an uncertainty associated with the necessity of taking into account the wall reactions, which are insufficiently studied. For long times and low pressures, the wall reactions can be represented in calculations as unimolecular reactions of the decay of species [reactions (140)–(143)].

1. Acetaldehyde

a. Two regions of the negative temperature coefficient

Acetaldehyde is a convenient subject for studying individual stages of the oxidation processes because its oxidation involves the appearance of intense cool and blue flames. Separate propagation of the latter was even observed at the initial room temperature.

Acetaldehyde oxidation was discussed in many studies (e.g., see monographs²⁻⁴ and references therein and also a recent paper²⁵); however, none of these publications described blue flames and the more so considered the possibility of their quantitative interpretation.

Kinetic schemes describing the oxidation of hydrocarbons C₁–C₂ were used²⁶ in modelling blue flames at the multistage

Table 1. Kinetic mechanism of oxidation and combustion of acetadehyde and hydrocarbons C₁–C₂.

Reaction number	Reaction	<i>H</i> /kJ mol ⁻¹	Forward reaction			Reverse reaction		
			<i>A</i> ^a	<i>n</i>	<i>E</i> /kJ mol ⁻¹	<i>A</i> ^a	<i>n</i>	<i>E</i> /kJ mol ⁻¹
1	OH + H ₂ ⇌ H + H ₂ O	62.80	2.2 × 10 ⁵	1.5	14.65	1.00 × 10 ⁶	1.5	77.87
2	OH + O ⇌ H + O ₂	66.99	2.8 × 10 ¹²	-0.8	-0.42	1.90 × 10 ¹¹	0.0	68.66
3	OH + H ⇌ O + H ₂	8.37	6.9 × 10 ⁹	0.0	29.31	1.50 × 10 ¹⁰	0.0	37.26
4	OH + OH ⇌ O + H ₂ O	71.18	6.0 × 10 ⁵	1.3	0.00	6.30 × 10 ⁶	1.3	71.18
5	H + H + M ⇌ H ₂ + M	431.24	2.0 × 10 ¹⁰	-0.3	0.00	1.00 × 10 ¹⁷	-1.3	438.78
6	O + O + M ⇌ O ₂ + M	494.04	3.6 × 10 ⁹	-0.6	0.00	1.60 × 10 ¹⁷	-1.6	502.42
7	OH + H + M ⇌ H ₂ O + M	494.04	3.6 × 10 ¹³	-1.0	0.00	8.70 × 10 ¹⁷	-2.0	502.42
8	O + H + M ⇌ OH + M	422.87	4.7 × 10 ⁹	0.0	0.00	1.1 × 10 ¹³	0.0	435.43
9	H + HO ₂ ⇌ H ₂ + O ₂	234.46	6.0 × 10 ⁹	0.0	0.00	1.1 × 10 ⁹	0.0	234.46
10	H + O ₂ + M ⇌ HO ₂ + M	196.78	4.1 × 10 ⁹	0.0	0.00	5.7 × 10 ¹²	0.0	204.32
11	H + HO ₂ ⇌ OH + OH	154.91	2.0 × 10 ¹⁰	0.0	0.00	1.6 × 10 ⁹	0.0	157.42
12	O + HO ₂ ⇌ O ₂ + OH	226.09	6.0 × 10 ¹⁰	0.0	0.00	9.4 × 10 ¹⁰	0.0	226.09
13	OH + HO ₂ ⇌ O ₂ + H ₂ O	297.26	6.0 × 10 ⁹	0.0	0.00	1.0 × 10 ¹¹	0.0	298.10
14	H + HO ₂ ⇌ H ₂ O + O	226.09	6.0 × 10 ⁸	0.0	0.00	5.3 × 10 ⁸	0.0	227.76
15	OH + H ₂ O ₂ ⇌ HO ₂ + H ₂ O	129.79	1.8 × 10 ⁹	0.0	1.26	1.9 × 10 ⁹	0.0	130.63
16	H + H ₂ O ₂ ⇌ H ₂ O + OH	276.13	7.1 × 10 ⁹	0.0	17.58	6.4 × 10 ⁸	0.0	303.96
17	OH + OH + M ⇌ H ₂ O ₂ + M	209.34	1.6 × 10 ⁸	0.0	-40.19	4.1 × 10 ¹³	0.0	175.85
18	O + H ₂ O ₂ ⇌ O ₂ + H ₂ O	355.88	2.8 × 10 ¹⁰	0.0	26.80	4.8 × 10 ¹⁰	0.0	382.67
19	H + H ₂ O ₂ ⇌ H ₂ + HO ₂	66.99	7.00 × 10 ⁹	0.0	17.58	1.6 × 10 ⁹	0.0	83.74
20	HO ₂ + HO ₂ ⇌ H ₂ O ₂ + O ₂	167.47	2.4 × 10 ¹⁰	0.0	6.28	3.7 × 10 ¹¹	0.0	175.01
21	O + H ₂ O ₂ ⇌ HO ₂ + OH	58.62	2.8 × 10 ¹⁰	0.0	26.80	2.9 × 10 ⁹	0.0	85.41
22	CO + OH ⇌ CO ₂ + H	108.86	1.2 × 10 ⁴	1.4	-1.67	4.6 × 10 ⁶	1.4	101.32
23	CO + HO ₂ ⇌ CO ₂ + OH	259.58	1.3 × 10 ¹¹	0.0	96.30	4.3 × 10 ¹²	0.0	355.88
24	CO + O + M ⇌ CO ₂ + M	531.72	6.2 × 10 ⁸	0.0	12.56	4.7 × 10 ¹⁴	0.5	548.47

Table 1 (continued).

Reaction number	Reaction	$H/\text{kJ mol}^{-1}$	Forward reaction			Reverse reaction		
			A^a	n	$E/\text{kJ mol}^{-1}$	A^a	n	$E/\text{kJ mol}^{-1}$
25	$\text{CO} + \text{O}_2 \rightleftharpoons \text{CO}_2 + \text{O}$	37.68	2.5×10^9	0.0	200.97	5.1×10^{10}	0.0	234.46
26	$\text{HCHO} + \text{OH} \rightleftharpoons \text{HCO} + \text{H}_2\text{O}$	121.42	7.5×10^9	0.0	0.84	2.2×10^9	0.0	121.42
27	$\text{HCHO} + \text{H} \rightleftharpoons \text{HCO} + \text{H}_2$	58.62	6.0×10^{10}	0.0	6.28	3.7×10^9	0.0	64.90
28	$\text{HCHO} + \text{O} \rightleftharpoons \text{HCO} + \text{OH}$	50.24	1.8×10^{10}	0.0	12.98	5.0×10^8	0.0	63.64
29	$\text{HO}_2 + \text{HCO} \rightleftharpoons \text{HCHO} + \text{O}_2$	171.66	3.5×10^8	0.0	52.34	2.0×10^{10}	0.0	222.32
30	$\text{H} + \text{CO} + \text{M} \rightleftharpoons \text{HCO} + \text{M}$	62.80	1.2×10^8	0.0	2.51	1.9×10^{14}	-1.0	71.18
31	$\text{H}_2\text{O}_2 + \text{HCO} \rightleftharpoons \text{HCHO} + \text{HO}_2$	12.56	1.6×10^8	0.0	20.93	6.0×10^8	0.0	33.49
32	$\text{HCO} + \text{O}_2 \rightleftharpoons \text{HO}_2 + \text{CO}$	142.35	6.0×10^{10}	0.0	30.14	5.5×10^{10}	0.0	173.75
33	$\text{O} + \text{HCO} \rightleftharpoons \text{H} + \text{CO}_2$	468.92	1.2×10^9	0.0	0.00	6.8×10^{11}	0.0	468.92
34	$\text{HCO} + \text{H} + \text{M} \rightleftharpoons \text{HCHO} + \text{M}$	376.81	3.8×10^4	1.0	0.00	3.2×10^{12}	0.0	314.01
35	$\text{OH} + \text{HCO} \rightleftharpoons \text{CO} + \text{H}_2\text{O}$	435.43	6.0×10^{10}	0.0	0.00	8.9×10^{11}	0.0	435.43
36	$\text{H} + \text{HCO} \rightleftharpoons \text{H}_2 + \text{CO}$	372.63	6.0×10^{10}	0.0	0.00	1.9×10^{11}	0.0	372.63
37	$\text{O} + \text{HCO} \rightleftharpoons \text{OH} + \text{CO}$	364.25	6.0×10^8	0.0	0.00	8.5×10^8	0.0	364.25
38	$\text{OH} + \text{CH}_4 \rightleftharpoons \text{CH}_3 + \text{H}_2\text{O}$	71.18	1.6×10^4	1.8	11.72	1.8×10^3	1.8	79.13
39	$\text{CH}_3 + \text{H}_2 \rightleftharpoons \text{H} + \text{CH}_4$	4.19	1.9×10^9	0.0	46.05	7.6×10^{10}	0.0	50.24
40	$\text{OH} + \text{CH}_3 \rightleftharpoons \text{O} + \text{CH}_4$	8.37	7.6×10^3	1.6	25.12	6.9×10^5	1.6	35.59
41	$\text{HO}_2 + \text{CH}_3 \rightleftharpoons \text{O}_2 + \text{CH}_4$	226.09	4.3×10^8	0.0	-1.67	6.0×10^{10}	0.0	230.27
42	$\text{H} + \text{CH}_3 + \text{M} \rightleftharpoons \text{CH}_4 + \text{M}$	422.87	2.3×10^6	1.0	-45.64	4.7×10^{14}	0.0	391.88
43	$\text{CH}_3 + \text{H}_2\text{O}_2 \rightleftharpoons \text{HO}_2 + \text{CH}_4$	58.62	6.5×10^7	0.0	18.00	6.0×10^8	0.0	79.55
44	$\text{CH}_3 + \text{HCHO} \rightleftharpoons \text{HCO} + \text{CH}_4$	62.80	1.0×10^9	0.0	18.84	2.5×10^9	0.0	79.97
45	$\text{HCO} + \text{CH}_3 \rightleftharpoons \text{CO} + \text{CH}_4$	376.81	6.0×10^{10}	0.0	0.00	7.8×10^{12}	0.0	374.72
46	$\text{O} + \text{CH}_3\text{O} \rightleftharpoons \text{CH}_3 + \text{O}_2$	117.23	1.7×10^{11}	0.0	12.14	2.3×10^{10}	0.0	128.95
47	$\text{OH} + \text{CH}_3 \rightleftharpoons \text{CH}_2 + \text{H}_2\text{O}$	37.68	6.0×10^9	0.0	11.72	2.2×10^{10}	0.0	50.24
48	$\text{O} + \text{CH}_2 \rightleftharpoons \text{H} + \text{HCO}$	376.81	6.0×10^9	0.0	0.00	4.5×10^{10}	0.0	376.81
49	$\text{CH}_2 + \text{H}_2\text{O} \rightleftharpoons \text{H}_2 + \text{HCHO}$	263.77	6.0×10^9	0.0	10.47	3.5×10^{11}	0.0	273.82
50	$\text{CH}_2 + \text{O}_2 \rightleftharpoons \text{OH} + \text{H} + \text{CO}$	247.02	6.0×10^9	0.0	14.65	1.5×10^3	1.0	256.23
51	$\text{CH}_2 + \text{O}_2 \rightleftharpoons \text{H} + \text{H} + \text{CO}_2$	351.69	1.8×10^8	0.0	0.00	1.8×10^4	1.0	343.32
52	$\text{CH}_3 + \text{O}_2 \rightleftharpoons \text{OH} + \text{HCHO}$	213.53	4.0×10^9	0.0	75.36	3.8×10^9	0.0	288.89
53	$\text{O} + \text{CH}_3 \rightleftharpoons \text{H} + \text{HCHO}$	284.70	7.2×10^{10}	0.0	0.00	1.5×10^{12}	0.0	285.54
54	$\text{CH}_3 + \text{O}_2 \rightleftharpoons \text{CH}_3\text{O}_2$	117.23	6.0×10^8	0.0	0.00	5.0×10^{13}	0.0	131.47
55	$\text{OH} + \text{CH}_3\text{O} \rightleftharpoons \text{CH}_3\text{O}_2\text{H}$	180.03	6.0×10^{10}	0.0	0.00	1.0×10^{15}	0.0	180.03
56	$\text{HO}_2 + \text{CH}_3 \rightleftharpoons \text{H}_2\text{O} + \text{HCHO}$	510.79	1.2×10^9	0.0	0.00	1.2×10^9	0.0	510.79
57	$\text{CH}_3\text{O}_2\text{H} + \text{CH}_3 \rightleftharpoons \text{CH}_3\text{O}_2 + \text{CH}_4$	62.80	6.0×10^8	0.0	19.68	6.0×10^8	0.0	83.74
58	$\text{OH} + \text{CH}_2 \rightleftharpoons \text{H}_2\text{O} + \text{CH}$	75.33	6.0×10^9	0.0	29.30	1.4×10^{10}	0.0	104.63
59	$\text{H} + \text{CH}_2 \rightleftharpoons \text{H}_2 + \text{CH}$	12.56	6.0×10^9	0.0	46.05	3.1×10^9	0.0	56.52
60	$\text{O} + \text{CH}_2 \rightleftharpoons \text{OH} + \text{CH}$	4.19	6.0×10^9	0.0	46.05	1.4×10^9	0.0	50.24
61	$\text{OH} + \text{CH} \rightleftharpoons \text{H}_2 + \text{CO}$	741.06	6.0×10^9	0.0	0.00	6.2×10^{11}	0.0	749.44
62	$\text{O} + \text{CH} \rightleftharpoons \text{H} + \text{CO}$	732.69	6.0×10^9	0.0	0.00	2.8×10^{11}	0.0	741.06
63	$\text{OH} + \text{CH}_3 \rightleftharpoons \text{CH}_3\text{OH}$	385.19	9.4×10^6	1.0	-9.21	9.4×10^{15}	0.0	376.81
64	$\text{HO}_2 + \text{CH}_3\text{O} \rightleftharpoons \text{CH}_3\text{OH} + \text{O}_2$	226.09	2.6×10^8	0.0	0.00	6.0×10^9	0.0	217.71
65	$\text{CH}_3\text{O} + \text{CH}_4 \rightleftharpoons \text{CH}_3\text{OH} + \text{CH}_3$	0.00	4.7×10^8	0.0	37.26	1.4×10^8	0.0	46.89
66	$\text{OH} + \text{CH}_3\text{OH} \rightleftharpoons \text{H}_2\text{O} + \text{CH}_3\text{O}$	71.18	6.0×10^9	0.0	30.14	4.7×10^9	0.0	96.30
67	$\text{H} + \text{CH}_3\text{OH} \rightleftharpoons \text{H}_2 + \text{CH}_3\text{O}$	8.37	1.3×10^{10}	0.0	22.19	2.2×10^9	0.0	25.54
68	$\text{O} + \text{CH}_3\text{OH} \rightleftharpoons \text{OH} + \text{CH}_3\text{O}$	0.00	4.3×10^9	0.0	8.37	3.2×10^8	0.0	4.19
69	$\text{CH}_3\text{O} + \text{O}_2 \rightleftharpoons \text{HO}_2 + \text{H}_2\text{CO}$	104.67	6.6×10^7	0.0	10.89	2.8×10^8	0.0	125.60
70	$\text{H} + \text{H}_2\text{CO} + \text{M} \rightleftharpoons \text{CH}_3\text{O} + \text{M}$	92.11	1.2×10^5	1.0	26.80	6.0×10^{11}	0.0	92.11
71	$\text{OH} + \text{CH}_3\text{O} \rightleftharpoons \text{H}_2\text{O} + \text{HCHO}$	401.93	6.0×10^9	0.0	0.00	8.3×10^9	0.0	401.93
72	$\text{H} + \text{CH}_3\text{O} \rightleftharpoons \text{H}_2 + \text{HCHO}$	339.13	6.0×10^{10}	0.0	0.00	1.8×10^{10}	0.0	339.13
73	$\text{O} + \text{CH}_3\text{O} \rightleftharpoons \text{OH} + \text{HCHO}$	330.76	6.0×10^9	0.0	0.00	7.9×10^8	0.0	332.43
74	$\text{O}_2 + \text{C}_2\text{H}_2 \rightleftharpoons \text{HCO} + \text{HCO}$	138.16	1.9×10^{11}	0.0	138.16	2.7×10^9	0.0	276.33
75	$\text{C}_2\text{H} + \text{H} + \text{M} \rightleftharpoons \text{C}_2\text{H}_2 + \text{M}$	523.35	6.8×10^5	1.0	-54.43	4.2×10^{13}	0.0	447.99
76	$\text{C}_2\text{H} + \text{H}_2 \rightleftharpoons \text{C}_2\text{H}_2 + \text{H}$	92.11	3.5×10^8	0.0	-2.51	6.0×10^9	0.0	83.74
77	$\text{C}_2\text{H} + \text{O}_2 \rightleftharpoons \text{CO} + \text{HCO}$	665.70	6.0×10^9	0.0	0.00	5.4×10^9	0.0	665.70
78	$\text{OH} + \text{C}_2\text{H}_2 \rightleftharpoons \text{CH}_3 + \text{CO}$	234.46	7.8×10^9	0.0	19.26	5.9×10^9	0.0	259.58
79	$\text{O} + \text{C}_2\text{H}_2 \rightleftharpoons \text{CH}_2 + \text{CO}$	192.59	2.2×10^1	2.8	20.93	5.8	2.8	334.94
80	$\text{H} + \text{C}_2\text{H}_2 \rightleftharpoons \text{C}_2\text{H}_3$	167.47	5.5×10^9	0.0	10.05	2.6×10^{16}	-1.0	194.27
81	$\text{H}_2 + \text{C}_2\text{H}_2 \rightleftharpoons \text{C}_2\text{H}_4$	171.66	1.6×10^3	1.0	46.05	3.1×10^{11}	0.0	231.95
82	$\text{OH} + \text{CO} + \text{CH}_3 \rightleftharpoons \text{O}_2 + \text{C}_2\text{H}_4$	20.93	2.8×10^1	1.0	133.98	6.0×10^{10}	0.0	146.54
83	$\text{OH} + \text{C}_2\text{H}_4 \rightleftharpoons \text{H}_2\text{O} + \text{C}_2\text{H}_3$	62.80	6.0×10^9	0.0	3.77	1.4×10^9	0.0	72.85
84	$\text{H}_2 + \text{C}_2\text{H}_3 \rightleftharpoons \text{H} + \text{C}_2\text{H}_4$	4.19	5.8×10^8	0.0	53.59	6.0×10^9	0.0	50.24
85	$\text{O} + \text{C}_2\text{H}_4 \rightleftharpoons \text{HCO} + \text{CH}_3$	113.04	6.0×10^9	0.0	2.93	5.0×10^7	0.0	113.04
86	$\text{O}_2 + \text{C}_2\text{H}_3 \rightleftharpoons \text{HO}_2 + \text{C}_2\text{H}_2$	29.31	6.0×10^9	0.0	41.87	1.8×10^9	0.0	62.80

Table 1 (continued).

Reaction number	Reaction	$H/\text{kJ mol}^{-1}$	Forward reaction			Reverse reaction		
			A^a	n	$E/\text{kJ mol}^{-1}$	A^a	n	$E/\text{kJ mol}^{-1}$
87	$\text{OH} + \text{C}_2\text{H}_3 \rightleftharpoons \text{HCO} + \text{CH}_3$	138.16	6.0×10^9	0.0	0.00	1.5×10^9	0.0	150.72
88	$\text{OH} + \text{C}_2\text{H}_3 \rightleftharpoons \text{H}_2\text{O} + \text{C}_2\text{H}_2$	326.57	6.0×10^9	0.0	0.00	2.3×10^{10}	0.0	318.20
89	$\text{H} + \text{C}_2\text{H}_3 \rightleftharpoons \text{H}_2 + \text{C}_2\text{H}_2$	263.77	6.0×10^9	0.0	0.00	6.3×10^{10}	0.0	259.58
90	$\text{O} + \text{C}_2\text{H}_3 \rightleftharpoons \text{CH}_3 + \text{CO}$	489.86	6.0×10^9	0.0	0.00	2.1×10^9	0.0	485.67
91	$\text{O} + \text{C}_2\text{H}_3 \rightleftharpoons \text{OH} + \text{C}_2\text{H}_2$	255.39	6.0×10^9	0.0	0.00	2.8×10^9	0.0	251.21
92	$\text{CH}_4 + \text{C}_2\text{H}_3 \rightleftharpoons \text{CH}_3 + \text{C}_2\text{H}_4$	12.56	6.0×10^8	0.0	46.05	2.0×10^9	0.0	58.62
93	$\text{CH}_3 + \text{CH}_3 \rightleftharpoons \text{C}_2\text{H}_4 + \text{H}_2$	230.27	2.0×10^{13}	0.0	159.94	3.0×10^{15}	0.0	381.00
94	$\text{C}_2\text{H}_4 + \text{H} + \text{H} \rightleftharpoons \text{CH}_3 + \text{CH}_3$	200.97	1.8×10^6	1.0	-41.87	6.0×10^{10}	0.0	174.17
95	$\text{HCHO} + \text{C}_2\text{H}_3 \rightleftharpoons \text{HCO} + \text{C}_2\text{H}_4$	75.36	6.0×10^{10}	0.0	0.00	6.0×10^{10}	0.0	75.36
96	$\text{HCO} + \text{CH}_3 \rightleftharpoons \text{CH}_3\text{CHO}$	355.88	6.6×10^8	1.0	0.00	1.2×10^{16}	0.0	341.22
97	$\text{HO}_2 + \text{CH}_3\text{CO} \rightleftharpoons \text{CH}_3\text{CHO} + \text{O}_2$	154.91	5.3×10^7	0.0	0.00	1.0×10^9	0.0	163.29
98	$\text{OH} + \text{CH}_3\text{CHO} \rightleftharpoons \text{H}_2\text{O} + \text{CH}_3\text{CO}$	138.16	3.3×10^9	0.0	6.70	2.9×10^9	0.0	146.54
99	$\text{H} + \text{CH}_3\text{CHO} \rightleftharpoons \text{H}_2 + \text{CH}_3\text{CO}$	75.36	1.4×10^{10}	0.0	13.82	1.2×10^9	0.0	89.18
100	$\text{O} + \text{CH}_3\text{CHO} \rightleftharpoons \text{OH} + \text{CH}_3\text{CO}$	66.99	7.2×10^9	0.0	8.37	6.0×10^8	0.0	75.36
101	$\text{HO}_2 + \text{CH}_3\text{CHO} \rightleftharpoons \text{H}_2\text{O}_2 + \text{CH}_3\text{CO}$	4.19	6.0×10^8	0.0	41.87	4.9×10^8	0.0	46.05
102	$\text{CH}_3 + \text{CO} + \text{M} \rightleftharpoons \text{CH}_3\text{CO} + \text{M}$	58.62	1.1×10^8	0.0	15.91	6.0×10^{12}	0.0	59.45
103	$\text{H} + \text{CH}_3\text{CO} \rightleftharpoons \text{HCO} + \text{CH}_3$	4.19	6.0×10^9	0.0	20.10	6.6×10^7	0.0	26.38
104	$\text{O} + \text{CH}_3\text{CO} \rightleftharpoons \text{CO} + \text{CH}_3\text{O}$	322.38	6.0×10^9	0.0	0.00	1.6×10^{10}	0.0	322.38
105	$\text{C}_2\text{H}_5 + \text{O}_2 \rightleftharpoons \text{OH} + \text{CH}_3\text{CHO}$	255.39	4.0×10^9	0.0	75.36	3.0×10^9	0.0	330.76
106	$\text{HO}_2 + \text{C}_2\text{H}_5 \rightleftharpoons \text{O}_2 + \text{C}_2\text{H}_6$	213.53	3.2×10^8	0.0	-5.02	6.0×10^9	0.0	209.34
107	$\text{CH}_3 + \text{CH}_3 \rightleftharpoons \text{C}_2\text{H}_6$	376.81	8.4×10^9	0.0	0.00	1.3×10^{16}	0.0	364.25
108	$\text{OH} + \text{C}_2\text{H}_6 \rightleftharpoons \text{H}_2\text{O} + \text{C}_2\text{H}_5$	83.74	1.8×10^{11}	0.0	16.75	1.6×10^{11}	0.0	100.48
109	$\text{H} + \text{C}_2\text{H}_6 \rightleftharpoons \text{H}_2 + \text{C}_2\text{H}_5$	20.93	7.4×10^{10}	0.0	40.19	1.4×10^{10}	0.0	59.45
110	$\text{O} + \text{C}_2\text{H}_6 \rightleftharpoons \text{OH} + \text{C}_2\text{H}_5$	12.56	4.6×10^9	0.0	16.75	3.8×10^8	0.0	29.31
111	$\text{H}_2\text{O}_2 + \text{C}_2\text{H}_5 \rightleftharpoons \text{HO}_2 + \text{C}_2\text{H}_6$	46.05	4.9×10^8	0.0	33.49	6.0×10^8	0.0	79.55
112	$\text{H} + \text{C}_2\text{H}_4 \rightleftharpoons \text{C}_2\text{H}_5$	138.16	8.8×10^{10}	-0.5	5.86	1.1×10^{14}	-0.6	160.35
113	$\text{C}_2\text{H}_5 + \text{O}_2 \rightleftharpoons \text{HO}_2 + \text{C}_2\text{H}_4$	58.62	6.0×10^8	0.0	33.49	4.5×10^7	0.0	75.36
114	$\text{C}_2\text{H}_5 + \text{O}_2 \rightleftharpoons \text{HCHO} + \text{CH}_3\text{O}$	230.27	6.0×10^8	0.0	41.87	1.7×10^8	0.0	259.58
115	$\text{OH} + \text{C}_2\text{H}_5 \rightleftharpoons \text{CH}_3 + \text{CH}_3\text{O}$	16.75	3.0×10^{10}	0.0	0.00	8.0×10^9	0.0	5.86
116	$\text{OH} + \text{C}_2\text{H}_5 \rightleftharpoons \text{H}_2\text{O} + \text{C}_2\text{H}_4$	355.88	6.0×10^9	0.0	0.00	7.2×10^9	0.0	334.94
117	$\text{H} + \text{C}_2\text{H}_5 \rightleftharpoons \text{CH}_3 + \text{CH}_3$	62.80	4.8×10^{10}	0.0	4.61	8.2×10^7	0.0	53.59
118	$\text{H} + \text{C}_2\text{H}_5 \rightleftharpoons \text{CH}_2 + \text{CH}_4$	20.93	6.0×10^9	0.0	25.12	7.1×10^7	0.0	40.19
119	$\text{H} + \text{C}_2\text{H}_5 \rightleftharpoons \text{C}_2\text{H}_6$	410.31	3.6×10^{10}	0.0	0.00	1.0×10^{15}	0.0	410.31
120	$\text{H} + \text{C}_2\text{H}_5 \rightleftharpoons \text{H}_2 + \text{C}_2\text{H}_4$	293.08	6.0×10^9	0.0	0.00	1.6×10^9	0.0	276.33
121	$\text{O} + \text{C}_2\text{H}_5 \rightleftharpoons \text{CH}_3 + \text{H}_2\text{CO}$	347.50	6.0×10^{10}	0.0	0.00	2.1×10^8	0.0	334.94
122	$\text{O} + \text{C}_2\text{H}_5 \rightleftharpoons \text{OH} + \text{C}_2\text{H}_4$	284.70	6.0×10^9	0.0	0.00	6.9×10^8	0.0	267.96
123	$\text{H}_2 + \text{C}_2\text{H} \rightleftharpoons \text{H} + \text{C}_2\text{H}_2$	117.23	3.5×10^8	0.0	-20.93	6.0×10^9	0.0	83.74
124	$\text{CH}_3\text{O}_2 + \text{CH}_3 \rightleftharpoons \text{CH}_3\text{O} + \text{CH}_3\text{O}$	142.35	1.3×10^9	0.0	0.00	2.9×10^9	0.0	142.35
125	$\text{CH}_3\text{O}_2 + \text{HO}_2 \rightleftharpoons \text{CH}_3\text{O}_2\text{H} + \text{O}_2$	167.47	5.0×10^7	0.0	12.56	6.8×10^8	0.0	180.03
126	$\text{CH}_3 + \text{HO}_2 \rightleftharpoons \text{CH}_3\text{O} + \text{OH}$	108.86	2.0×10^8	0.0	0.00	2.0×10^9	0.0	117.23
127	$\text{C}_2\text{H}_5 + \text{O}_2 \rightleftharpoons \text{C}_2\text{H}_5\text{O}_2$	117.23	2.8×10^7	0.0	-4.19	2.0×10^{14}	-1.0	104.67
128	$\text{C}_2\text{H}_5\text{O}_2\text{H} + \text{C}_2\text{H}_5 \rightleftharpoons \text{C}_2\text{H}_5\text{O}_2 + \text{C}_2\text{H}_6$	20.93	1.8×10^7	0.0	50.24	6.3×10^8	0.0	71.18
129	$\text{C}_2\text{H}_5\text{O} + \text{OH} \rightleftharpoons \text{C}_2\text{H}_5\text{O}_2\text{H}$	180.03	5.5×10^7	1.0	16.33	4.0×10^{15}	0.0	180.03
130	$\text{C}_2\text{H}_4 + \text{OH} \rightleftharpoons \text{C}_2\text{H}_5\text{O}$	100.48	9.1×10^6	1.0	8.37	1.3×10^{13}	0.0	108.86
131	$\text{CH}_3 + \text{HCHO} \rightleftharpoons \text{C}_2\text{H}_5\text{O}$	46.05	5.0×10^7	1.0	41.87	1.0×10^{14}	0.0	87.92
132	$\text{C}_2\text{H}_5\text{O}_2 + \text{C}_2\text{H}_5 \rightleftharpoons \text{C}_2\text{H}_5\text{O} + \text{C}_2\text{H}_5\text{O}$	129.79	6.3×10^8	0.0	0.00	1.1×10^8	0.0	126.02
133	$\text{C}_2\text{H}_5\text{O}_2 + \text{HO}_2 \rightleftharpoons \text{C}_2\text{H}_5\text{O}_2\text{H} + \text{O}_2$	163.29	7.9×10^7	0.0	8.37	3.7×10^8	0.0	171.66
134	$\text{C}_2\text{H}_5 + \text{HO}_2 \rightleftharpoons \text{C}_2\text{H}_5\text{O} + \text{OH}$	104.67	2.0×10^8	0.0	0.00	1.2×10^7	0.0	104.67
135	$\text{CH}_3\text{CO} + \text{O}_2 \rightleftharpoons \text{CH}_3\text{CO}_3$	117.23	1.0×10^9	0.0	0.00	1.0×10^{14}	0.0	117.23
136	$\text{CH}_3\text{CO}_3 + \text{CH}_3\text{CHO} \rightleftharpoons \rightleftharpoons \text{CH}_3\text{CO} + \text{CH}_3\text{CO}_3\text{H}$	8.37	6.3×10^8	0.0	35.59	1.8×10^7	0.0	43.96
137	$\text{CH}_3 + \text{CO}_2 + \text{OH} \rightleftharpoons \text{CH}_3\text{CO}_3\text{H}$	138.16	5.5×10^4	2.0	0.00	6.0×10^{14}	0.0	138.16
138	$\text{CH}_3\text{CO}_3 + \text{HO}_2 \rightleftharpoons \text{CH}_3\text{CO}_3\text{H} + \text{O}_2$	167.47	7.9×10^7	0.0	0.00	3.7×10^8	0.0	167.47
139	$\text{CH}_3\text{O}_2 + \text{CH}_3\text{CHO} \rightleftharpoons \rightleftharpoons \text{CH}_3\text{CO} + \text{CH}_3\text{O}_2\text{H}$	12.56	6.0×10^8	0.0	62.80	6.8×10^8	0.0	75.36
140	$\text{H}_2\text{O}_2 \longrightarrow \text{H}_2\text{O} + 0.5\text{O}_2$	0.00	3.0	0.0	0.00			
141	$\text{CH}_3\text{OOH} \longrightarrow \text{H}_2 + \text{H}_2\text{O} + \text{CO}$	0.00	6.0	0.0	0.00			
142	$\text{CH}_3\text{COOOH} \longrightarrow \text{CO} + \text{O}_2 + \text{CH}_4$	0.00	6.0	0.0	0.00			
143	$\text{C}_2\text{H}_5\text{OOH} \longrightarrow \text{H}_2\text{O} + \text{O}_2 + \text{CH}_4$	0.00	6.0	0.0	0.00			

^a A is the pre-exponential factor in equation describing the unimolecular (in s^{-1}), bimolecular ($\text{litre mol}^{-1} \text{s}^{-1}$) and trimolecular ($\text{litre}^2 \text{mol}^{-2} \text{s}^{-1}$) reactions.

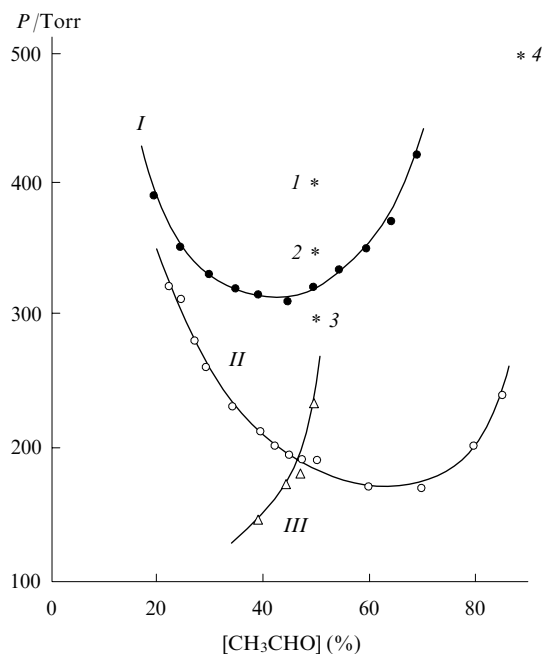


Figure 6. Regions of propagation of cool and blue flames (region I), only cool flame (II) and normal hot flame (III) in $\text{CH}_3\text{CHO} + \text{O}_2$ mixtures.⁸

Arabic numerals correspond to the conditions (pressure and mixture composition) under which solutions of the problem of propagation of normal hot flame (1, 2), cool flame (3) and combined propagation of cool and blue flame (4) were found.

autoignition of acetaldehyde mixtures with oxygen. Townend *et al.*⁸ have shown that in the induced ignition of 'rich' mixtures of diethyl ether and acetaldehyde with oxygen, one can observe cool and blue flames at reduced (subatmospheric) pressures and ambient or relatively low temperatures (Fig. 6), which involves only insignificant heating in the flames (50–250°) (cited according to Ref. 2). This is why before embarking on the kinetic modelling of blue flame, it is necessary to elucidate whether the region of acetaldehyde autoignition corresponds to the region of propagation of cool and blue flames upon ignition, how these flames are characterised and what are the calculated conditions of their origination. For these purposes, a kinetic scheme of the hydrocarbon C_1 – C_2 oxidation²⁷ supplemented by the data on acetaldehyde oxidation was taken.²⁸ Table 1 shows all the proposed elementary steps of acetaldehyde oxidation.

A homogeneous reaction (*i.e.*, a reaction that simultaneously proceeds in the whole reactor volume) in a closed vessel was modelled. A system of equation describing the material and heat balance in this reaction is as follows:

$$\frac{dn_j}{dt} = \sum_j w_{ij}, \quad (1)$$

$$\rho c_v \frac{dT}{dt} = \sum_j h_{ij} w_{ij} + \frac{\kappa S}{V} (T - T_w), \quad (2)$$

where n_j is the concentration of species; t is the time; T is the temperature; w_{ij} and h_{ij} are the rate and heat of the i th reaction (elementary step) involving the j th species; ρ is the density; c_v is the heat capacity at a constant volume; κ is the coefficient of heat-transfer to the walls of the reaction vessel; S and V are the surface and volume of the reaction vessel or a combustion chamber; T_w is the vessel wall temperature. The first term in Eqn (2) corresponds to the heat release due to the reaction, the second term corresponds to the heat exchange with the wall. The density was calculated using the equation of gas state. The

solution of this equation for the initial conditions $t = 0$, $n_j = [n_j]_0$, $T = T_0$ allows one to describe the kinetics of homogeneous reactions, *i.e.* find the time dependences of the temperature and concentrations of all substances involved in this reaction.

Figure 7 shows the calculated kinetic dependences of temperature (a) and concentrations of starting compounds (b), most important intermediate compounds and radicals

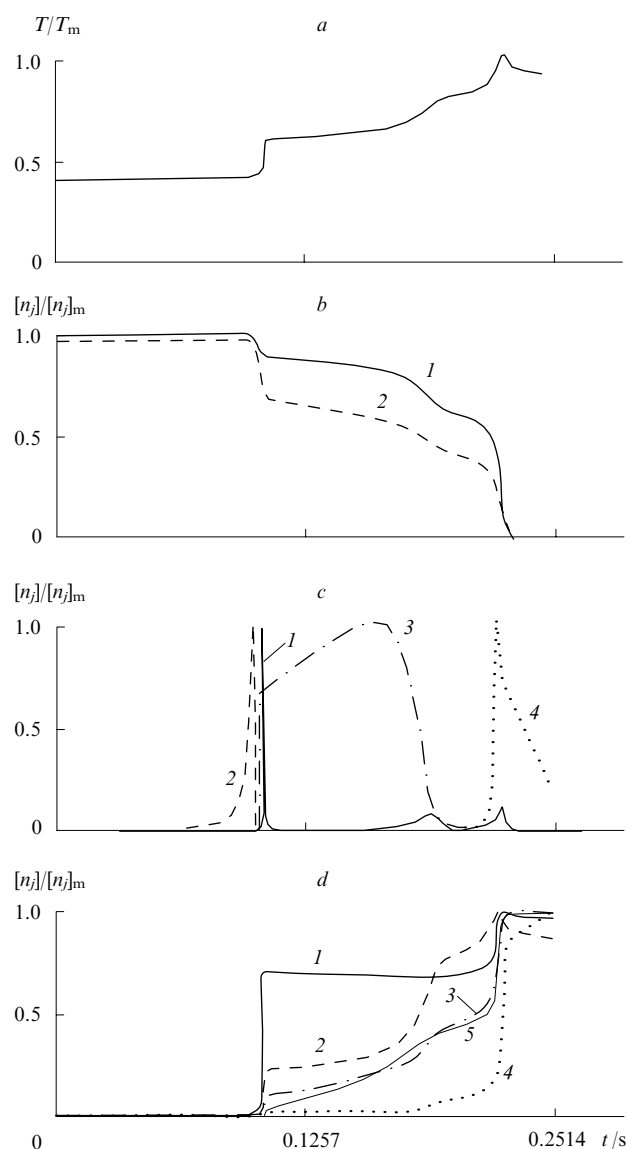


Figure 7. Time profiles of relative temperature (T/T_m , a) and concentrations $[n_j]/[n_j]_m$ (subscript m corresponds to the maximum values) of initial compounds (b), intermediate compounds and radicals (c) and also final products (d) at the autoignition of an acetaldehyde–oxygen mixture.²⁸ Initial conditions: $T_0 = 537$ K, $P_0 = 64.1$ kPa, $[\text{CH}_3\text{CHO}]_0 = 75\%$, $[\text{O}_2]_0 = 25\%$.

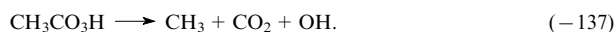
(a) T/T_m , $T_m = 1343$ K;

(b) (1) $[\text{CH}_3\text{CHO}]/[\text{CH}_3\text{CHO}]_m$, $[\text{CH}_3\text{CHO}]_m = 0.75$ (here and further, the maximum concentrations are given in volume fractions); (2) $[\text{O}_2]/[\text{O}_2]_m$, $[\text{O}_2]_m = 0.25$;

(c) (1) $[\text{OH}]/[\text{OH}]_m$, $[\text{OH}]_m = 8.55 \times 10^{-6}$, (2) $[\text{CH}_3\text{CO}_3\text{H}]/[\text{CH}_3\text{CO}_3\text{H}]_m$, $[\text{CH}_3\text{CO}_3\text{H}]_m = 1.27 \times 10^{-2}$; (3) $[\text{H}_2\text{O}_2]/[\text{H}_2\text{O}_2]_m$, $[\text{H}_2\text{O}_2]_m = 2.61 \times 10^{-2}$; (4) $[\text{H}]/[\text{H}]_m$, $[\text{H}]_m = 1.88 \times 10^{-5}$;

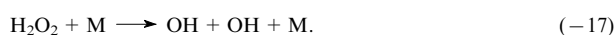
(d) (1) $[\text{CO}_2]/[\text{CO}_2]_m$, $[\text{CO}_2]_m = 3.67 \times 10^{-2}$; (2) $[\text{H}_2\text{O}]/[\text{H}_2\text{O}]_m$, $[\text{H}_2\text{O}]_m = 1.63 \times 10^{-1}$; (3) $[\text{CO}]/[\text{CO}]_m$, $[\text{CO}]_m = 4.02 \times 10^{-1}$; (4) $[\text{H}_2]/[\text{H}_2]_m$, $[\text{H}_2]_m = 2.33 \times 10^{-1}$; (5) $[\text{CH}_4]/[\text{CH}_4]_m$, $[\text{CH}_4]_m = 8.83 \times 10^{-2}$.

[CH₃CO₃H, H₂O₂, H, OH (*c*)] and final products [CO₂, CO, H₂, H₂O, CH₄ (*d*)] on time in the blue flame region for the autoignition of an acetaldehyde mixture ([CH₃CHO]₀ = 75%) with oxygen ([O₂]₀ = 25%). The calculations were carried out for the following initial conditions: $T_0 = 537$ K and $P_0 = 64.1$ kPa. The temperature curve (Fig. 7*a*) demonstrates three steps, which correspond to the temperature rise in cool, blue and conventional hot flames. The temperature rise in cool flame (at $t \approx 0.1$ s) is explained by a sharp increase in the reaction rate due to branching associated with the decomposition of hydroperoxide H₃CO₃H (hereinafter, the reaction number corresponds to that shown in Table 1).



The same time corresponds to the appearance of a maximum in the [OH]/[OH]_m vs. t curve (curve 1 in Fig. 7*c*).

In cool flame, a great deal of H₂O₂ is formed (curve 3 in Fig. 7*c*) the concentration of which first increases and then, after a certain period, starts to sharply decrease due to the H₂O₂ decomposition by the reaction



The second temperature jump due to the reaction acceleration as a result of the H₂O₂ decomposition is also accompanied by an increase in the concentration of OH radicals (the second peak in curve 1 in Fig. 7*c*). It is the chemical processes accompanying this temperature jump that are identified as the blue flame. The identification of blue flame and its mechanism as a local maximum of the reaction rate that arises due to the hydrogen peroxide decomposition was proposed in the study²⁹ dealing with analysis of the kinetics of ethane oxidation. The decomposition reaction of hydrogen peroxide is present in virtually all detailed kinetic schemes of hydrocarbon oxidation. However, before the appearance of the above publication,²⁹ the authors of these schemes never studied blue flames nor analysed their mechanism and the role of hydrogen peroxide decomposition in the appearance of blue flame.

Ultimately, as the reaction mixture is self-heated during the reaction, the conditions arise for the intense reaction branching typical of hot flames



which is accompanied by a new increase in the reaction rate and in the temperature. The concentrations of OH radicals (the third peak in curve 1, Fig. 7*c*) and hydrogen atoms H (curve 4 in Fig. 7*c*) increase again and the concentrations of acetaldehyde and oxygen decrease (curves 1 and 2 in Fig. 7*b*). Figure 7*d* shows the concentration profiles of several products of acetaldehyde oxidation and combustion, which are formed in the highest yields.

Presumably, the above description of the chemical process of acetaldehyde oxidation reflects the general phenomenological pattern and the essence of the three-stage autoignition of a CH₃CHO + O₂ mixture with the formation of cool, blue and hot flames.

Computations made it possible to follow the effect of the initial conditions (CH₃CHO + O₂ mixture composition, pressure and temperature) on the form of a $T(t)$ function, which describes most comprehensively the external aspects of a chemical reaction, in the t range from 0 to 0.5 s.²⁶ On the one hand, as the acetaldehyde concentration increases from 75% to 85%, the reaction rate decreases and the $T(t)$ function transforms from three-stage into two-stage due to the disappearance of the hot flame stage. On the other hand, the decrease in the [CH₃CHO]₀ concentration to 65% increases the reaction rate, and the three-step mechanism remains unchanged. With the

further decrease in the acetaldehyde concentration to 50%, the $T(t)$ function corresponds to a two-stage reaction that involves cool and hot flames. Thus, the form of the $T(t)$ function does not always one to conclude on the presence or absence of different stages during the acetaldehyde oxidation and also on the mechanism of relevant elementary reactions.

As the initial pressure of the gas mixture decreases from 64.1 to 25 kPa and the overall reaction decelerates, the function $T(t)$ transforms from three-stage into two-stage due to the disappearance of the hot-flame stage. At the pressure rise from 64.1 to 100 and 200 kPa, the function $T(t)$ still remains three-stage; however, further increase in the pressure to 400 and then to 1000 kPa results in the reaction acceleration and function $T(t)$ is no step-wise any longer.

The theory of oxidation and combustion of hydrocarbons uses the notion of induction period, which is the time during which the reaction rate increases to explosive without any visible indications. The description of a three-stage process³ involves the concepts of induction periods of cool (τ_1), blue (τ_2) and hot (τ_3) flames, where each period precedes a new increase in the temperature, and also a concept of the overall induction period $\tau_\Sigma = \tau_1 + \tau_2 + \tau_3$. The inflection points in the temperature curve $T(t)$ can be assumed conditionally to correspond to the end of period τ_1 and the beginning of period τ_2 and also the end of period τ_2 and the beginning of τ_3 . The values of τ_1 , τ_2 and τ_3 are largely qualitative estimates. To qualitatively assess the overall induction period τ_Σ , one may assume that it is equal to the time from the beginning of the process to the attainment of the maximum of function $T(t)$.

Basevich *et al.*²⁶ considered the dependence of calculated τ_Σ values on the initial temperature T_0 (Fig. 8). This Figure shows that in the range $T_0 = 500$ –1000 K, the $\tau_\Sigma(T)$ curve has two maxima (at $T_0 = 650$ and 900 K) and two minima (at $T_0 = 537$ and 775 K), *i.e.*, there are two NTC regions ($T_0 = 537$ –650 K and $T_0 = 775$ –900 K) in which the reaction rate decreases with an increase in the temperature.

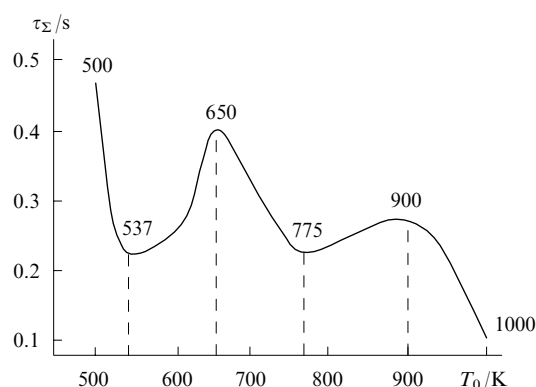


Figure 8. Dependences of the induction period on the initial temperature for autoignition of acetaldehyde mixtures with air at different temperatures.²⁶

Initial conditions: $P_0 = 64.1$ kPa, [CH₃CHO]₀ = 75%.

Figure 9 shows functions $T(t)$ obtained for different initial temperatures corresponding to such extrema in the τ_Σ vs. T_0 curve (see Fig. 8). It is evident that functions $T(t)$ are three-stage for $T_0 = 500$, 537 and 650 K, *i.e.*, in the vicinity of the first minimum (curves 1–3), two-stage without any apparent cool-flame stage for $T_0 = 775$ K (in the vicinity of the second minimum) (curve 4) and monotonically increase without any visible stages for $T_0 = 900$ and 1000 K (curves 5 and 6).

Such a shape of curves is explained by the fact that in the vicinity of the first minimum, three branching reactions occur,

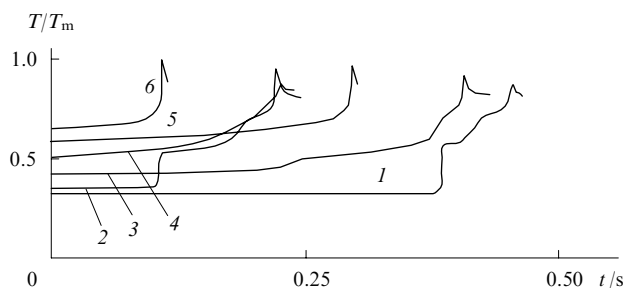
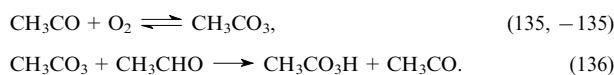
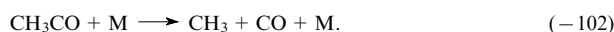


Figure 9. Time dependences of relative temperature for autoignition of acetaldehyde–oxygen mixtures at different initial temperatures.²⁶ T_0/K : (1) 500, (2) 537, (3) 650, (4) 775, (5) 900, (6) 1000. Initial conditions: $P_0 = 64.1$ kPa and $[\text{CH}_3\text{CHO}]_0 = 75\%$.

i.e., three-stage autoignition is observed. Hydroperoxide $\text{CH}_3\text{CO}_3\text{H}$ is formed in the reactions

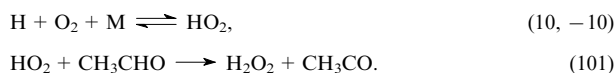


As the temperature increases (in the temperature range $T_0 = 537\text{--}650$ K), the equilibrium of reaction (135) shifts to the left and active decomposition of CH_3CO radicals by the following reaction begins:



As a result, the hydroperoxide concentration decreases, its decomposition by reaction (–137) does not play a significant role any longer, the rate of acetaldehyde oxidation decreases and the first NTC region appears.

A similar situation takes place in the temperature range $T_0 = 775\text{--}900$ K. At these initial temperatures, a large amount of hydrogen peroxide is formed



As the temperature increases, the equilibrium of reaction (10) shifts to the left. In this temperature range, reactions of consumption of hydrogen atoms start to prevail, the H_2O_2 concentration decreases, the branching of the acetaldehyde oxidation reaction due to the hydrogen peroxide decomposition [reaction (–17)] becomes insignificant and the process decelerates again, which is manifested by the appearance of the second NTC region.

With the further increase in the initial temperature, only one branching reaction remains, namely, the hydrogen atom reaction with oxygen (–2), which is typical of all high-temperature processes of hydrocarbon combustion. Now, function $T(t)$ increases monotonically.

Thus, the existence of two regions of the negative temperature coefficient of the reaction rate was theoretically proved for the first time.²⁶ Their existence was explained by the fact that the temperature range of the formation and decomposition of acetyl hydroperoxide (cool flames) is located much below the temperature range of hydrogen peroxide decomposition (blue flames) so that the cool and blue flames are well separated in time in the acetaldehyde autoignition.

b. Propagation of cool and blue flames

Data on the modelling of the propagation of cool flames through fresh unheated acetaldehyde mixtures with oxygen are available.²⁸ The calculations involved the use of a computer code³⁰ for solving the following system of equations that

describes the one-dimensional stationary propagation of the oxidation and combustion wave to be solved:³¹

$$\frac{\partial}{\partial x} \left[\rho D_j \frac{\partial (n_j/\rho)}{\partial x} \right] - \rho_0 u_n \frac{\partial (n_j/\rho)}{\partial x} + \sum_j w_{ij} = 0, \quad (3)$$

$$\frac{\partial}{\partial x} \left(\lambda \frac{\partial T}{\partial x} \right) - c_p \rho_0 u_n \frac{\partial T}{\partial x} + \sum_{ij} h_{ij} w_{ij} = 0, \quad (4)$$

where x is the coordinate along which the oxidation and combustion wave propagates; ρ , ρ_0 are the currently observed and initial densities, $\rho = \rho_0(T_0/T)(P/P_0)$; D_j is the diffusion coefficient of the j th species of the chemical reaction, $D_j = D_j^*(T/T^*)^{\gamma_j^2}(P/P^*)$ (the asterisk marks the parameters at normal conditions, $T^* = 293$ K and $P^* = 100$ kPa); u_n is the stationary velocity of wave propagation; λ is the molecular heat conductivity coefficient, $\lambda = \lambda^*(T/T^*)^{\gamma_\lambda^1}$; c_p is the specific heat, $c_p = c^* + c^{**}T$, where c^* , c^{**} , γ_λ^1 , γ_j^2 are constants.

The wave propagation velocity was determined based on the condition that the system of equations (3) and (4) has a solution at the following boundary conditions:

$$x \rightarrow -\infty: T \rightarrow T_0, \quad n_j \rightarrow [n_j]_0;$$

$$x \rightarrow +\infty: \frac{dT}{dx} \rightarrow 0, \quad \frac{d(n_j/\rho)}{dx} \rightarrow 0.$$

All the necessary coefficients were taken from reference editions.

The problem was solved using the relaxation method where the terms with derivative with respect to time (t) were added artificially to equations (3) and (4). After setting certain initial functions $T(t=0, x)$ and $n_j(t=0, x)$, the calculations were carried on up to a t value at which the temperature and concentration profiles and the u_n value no longer depended on time. As a result, a stationary solution to the non-stationary problem was found. This stationary solution is in fact quasistationary, because the calculations were stopped when the criteria of sufficiently small changes in temperature and concentration with time were fulfilled.

For a conventional 'hot' laminar flame, the stationarity means approaching the thermodynamic equilibrium. For cool and blue flames, there is no thermodynamic equilibrium: there is also no equilibrium in the initial fuel–oxidant mixture, but there exists a quasi-equilibrium that can be retained infinitely long. Apparently, depending on the form of initial functions [mainly depending on the function $T(t=0, x)$ at the right boundary], under conditions close to experimental,⁸ it is possible to find solutions that well describe both cool flame or cool and blue flames, on the one hand [if function $T(t=0, x)$ corresponds to the temperature of cool flame or cool and blue flames], and hot flame, on the other hand [if function $T(t=0, x)$ corresponds to the final equilibrium temperature of combustion].

Calculations²⁸ were carried out for different fuel–oxygen mixtures, the initial temperature $T_0 = 293$ K and several pressures. Profiles of temperature and substance concentrations in the propagating cool flame were reported²⁸ for an equimolar $\text{CH}_3\text{CHO} + \text{O}_2$ mixture at a pressure of 40 kPa (300 mm Hg). For this pressure, the flame propagation velocity was found to be equal to 2.4 cm s^{–1}. In cool flame, the temperature increased from 293 to 772 K. There, nearly 23% of starting reactants were consumed to afford a certain amount of stable products such as H_2 , H_2O , CO , CH_4 , etc. The rapid temperature increase in cool flame corresponds to a considerable increase in the concentration of the OH radical, one of the main active species in this reaction. This jump in the OH concentration coincides with a sharp decrease in the concentration of acetyl hydroperoxide $\text{CH}_3\text{CO}_3\text{H}$. The subsequent

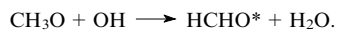
deceleration of the reaction with the decrease in the $[\text{OH}]$ was associated with the decomposition of secondary peroxides $\text{C}_2\text{H}_5\text{O}_2\text{H}$ and $\text{CH}_3\text{O}_2\text{H}$, which are more stable than $\text{CH}_3\text{CO}_3\text{H}$.

The appearance and joint propagation of cool and blue flames in a $\text{CH}_3\text{CHO} + \text{O}_2$ mixture was modelled.³² The first attempts to model blue flames failed due to the instability of the solution. However, this instability was overcome by refining the computation procedure.

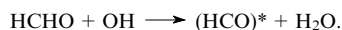
The calculations were carried out for $\text{CH}_3\text{CHO} + \text{O}_2$ mixtures with different composition, the initial temperature $T_0 = 293$ K and several pressures. In Fig. 6, the mixture compositions and pressures used in calculations are marked with asterisks. By selecting the initial functions for calculations, it was possible to simulate the flame types observed in experiments.

Let us consider a solution that corresponds to the joint propagation of cool and blue flames during the combustion of the 85% $\text{CH}_3\text{CHO} + 15\%$ O_2 mixture at a pressure of 67 kPa (point 4 in Fig. 6). Figure 10 shows the profiles of the temperature wave (T/T_m , *a*) and the concentration waves ($[n_i]/[n_i]_m$) of initial compounds (*b*), most important intermediate products and radicals (*c*) and final products (*d*), which contain separate zones of cool and blue flames. Under these initial conditions, the velocity of wave propagation was found to be 2.42 cm s^{-1} . Two temperature waves could be distinguished (see Fig. 10*a*). In cool flame, the temperature increased from 293 to 800 K, whereas in blue flame, it increased from 800 to 1267 K. The first temperature wave coincided with the decomposition of acetyl hydroperoxide $\text{CH}_3\text{CO}_3\text{H}$ to form OH radical and demonstrated a local maximum in the decay range. This maximum corresponds to the decomposition of secondary peroxides $\text{C}_2\text{H}_5\text{O}_2\text{H}$ and $\text{CH}_3\text{O}_2\text{H}$, which are somewhat more stable. The second temperature wave is associated with the decomposition of hydrogen peroxide H_2O_2 and HO_2 radicals to form OH radicals [due to the relatively large step of calculations over space, the resulting hydroxyl concentration curve is lumped rather than smooth (curve 4 in Fig. 7*c*)]. The following stable compounds were observed among the combustion products (in the order of decreasing concentration): H_2 , CH_4 , CO , H_2O , C_2H_4 , C_2H_6 , CO_2 , CH_3OH , *etc.* and the following radicals: CH_3 , HO_2 , CH_3O , C_2H_5 , CHO , OH , *etc.* Beyond the combustion zone, $\sim 10\%$ of acetaldehyde and more than 1% of oxygen remain non-consumed.

As was mentioned above, cool flame corresponds to the glow of excited HCHO^* . Apparently, this species is formed by the reaction



As is seen from Fig. 10*c*, the concentration profiles of methoxyl radical CH_3O and hydroxyl OH partly overlap, which corresponds to a certain probability that this reaction occurs in the cool flame zone. According to the same data, the blue flame glow owes its existence to the $(\text{HCO})^*$ radical. Presumably, this radical is formed by the reaction



Concentration profiles of HCHO and OH also overlap in the blue flame reaction zone, which shows that such a reaction can occur in this flame zone with a certain degree of probability.

The acetaldehyde oxidation mechanism assumed in a study²⁸ mentioned above includes none of these reactions, because the appearance of these species and their glow do not affect the main chemical process of heat release. In principle, the HCHO^* glow may be masked by the more intense $(\text{HCO})^*$ glow. The foregoing is nothing but the possible external manifestations of multistage mechanism of the acetaldehyde

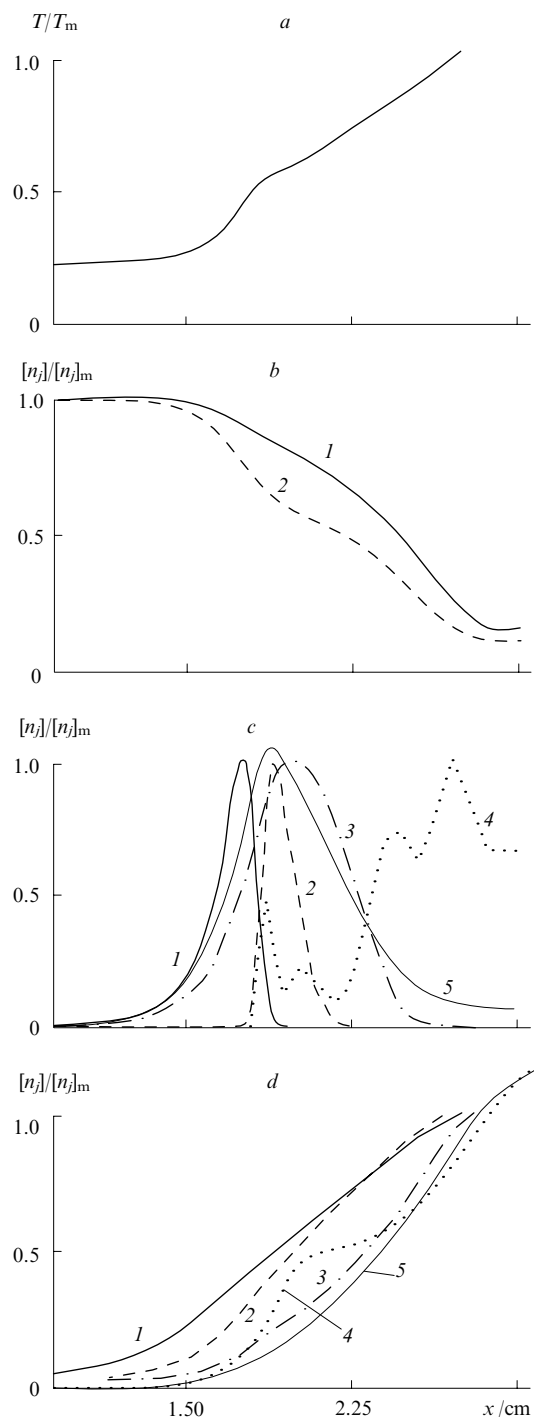


Figure 10. Profiles of relative temperature (T/T_m , *a*) and concentrations $[n_i]/[n_i]_m$ of initial compounds (*b*), most significant intermediate compounds and radicals (*c*) and final products (*d*) in the cool-flame reaction zone.³²

Initial conditions: $[\text{CH}_3\text{CHO}]_0 = 85\%$, $[\text{O}_2]_0 = 15\%$, $T_0 = 293$ K, $P_0 = 67$ kPa (~ 500 Torr).

(*a*) T/T_m , $T_m = 1267$ K;

(*b*) (1) $[\text{CH}_3\text{CHO}]/[\text{CH}_3\text{CHO}]_m$, $[\text{CH}_3\text{CHO}]_m = 0.85$; (2) $[\text{O}_2]/[\text{O}_2]_m$, $[\text{O}_2]_m = 0.15$;

(*c*) (1) $[\text{CH}_3\text{CO}_3\text{H}]/[\text{CH}_3\text{CO}_3\text{H}]_m$, $[\text{CH}_3\text{CO}_3\text{H}]_m = 1.7 \times 10^{-3}$; (2) $[\text{CH}_3\text{O}]/[\text{CH}_3\text{O}]_m$, $[\text{CH}_3\text{O}]_m = 4.5 \times 10^{-5}$; (3) $[\text{H}_2\text{O}_2]/[\text{H}_2\text{O}_2]_m$, $[\text{H}_2\text{O}_2]_m = 8.1 \times 10^{-3}$; (4) $[\text{OH}]/[\text{OH}]_m$, $[\text{OH}]_m = 1.4 \times 10^{-7}$; (5) $[\text{HCHO}]/[\text{HCHO}]_m$, $[\text{HCHO}]_m = 6.0 \times 10^{-3}$;

(*d*) (1) $[\text{H}_2]/[\text{H}_2]_m$, $[\text{H}_2]_m = 0.15$; (2) $[\text{H}_2\text{O}]/[\text{H}_2\text{O}]_m$, $[\text{H}_2\text{O}]_m = 0.0729$; (3) $[\text{CO}]/[\text{CO}]_m$, $[\text{CO}]_m = 0.401$; (4) $[\text{CO}_2]/[\text{CO}_2]_m$, $[\text{CO}_2]_m = 0.024$; (5) $[\text{CH}_4]/[\text{CH}_4]_m$, $[\text{CH}_4]_m = 0.135$.

oxidation and joint propagation of cool and blue flames. The presence of branching reactions in the decomposition of $\text{CH}_3\text{CO}_3\text{H}$ and H_2O_2 also points to the multistage nature of the acetaldehyde oxidation.

It can be stated that when cool and blue flames propagate in fresh unheated $\text{CH}_3\text{CHO} + \text{O}_2$ mixtures, the cool-flame and blue-flame reactions follow the same route as in the appearance of conventional bulk homogeneous cool and blue flames, with a difference that these reactions are initiated by the heat transfer and diffusion and such a double flame propagates over initially unheated mixtures.

The solutions corresponding to the propagating hot flame were not analysed in the mentioned study.²⁸

2. n-Heptane

Well-pronounced blue flame was observed in the combustion of n-heptane. Sokolik and Yantovskii³ experimentally (by recording the pressure) proved the multistage mechanism of the combustion of an n-heptane–air mixture in a closed vessel. The experiment was carried out at the relatively low initial temperature $T_0 = 573$ K and pressure $P_0 = 150$ kPa. The authors observed three pressure waves, namely, the first cool-flame wave, the second blue-flame wave and the third wave corresponding to the hot explosion (Fig. 11). In Fig. 11, the waves of cool and blue flames are united in a single delay τ_2 . This is associated with the fact that the authors have not yet brought forth a concept of multistage autoignition and

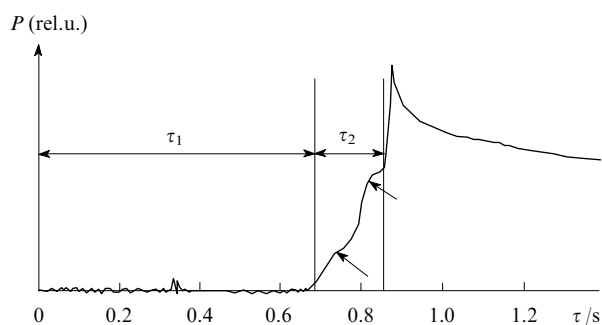


Figure 11. Pressure changes at autoignition of an n-heptane–air mixture with stoichiometric ratio $\phi = 1.25$. Initial conditions: $T_0 = 573$ K, $P_0 = 150$ kPa.³

explained the observed pressure jumps based on another idea.

A semi-empirical mechanism of n-heptane oxidation and combustion at the higher initial temperature (700–1300 K) and pressure (1200–10 000 kPa) was proposed and checked in a series of calculations that modelled the autoignition and combustion of n-heptane in propagating flame.³³ Figure 12 shows the autoignition delay times, both experimental and calculated based on the kinetic mechanism of n-heptane autoignition (for the experimental data on the overall autoignition delays $\tau_\Sigma = \tau_1 + \tau_2 + \tau_3$, see Ref. 33). It is evident that the results of calculations adequately agree with experimental data. Modelling of n-heptane oxidation and combustion has shown³⁴ that the proposed³³ kinetic mechanism of this process describes rather adequately the multistage autoignition of n-heptane with the appearance of cool and blue flames. The conditions taken in calculations corresponded to experimental conditions (stoichiometric amounts of n-heptane and air, $P_0 = 1500$ kPa) and the temperature range embraced an interval from 680 to 1000 K (the temperature corresponding to the beginning of high-temperature oxidation). Figure 13 shows the results of calculations. The calculations demonstrated the time dependences (in the range of the overall

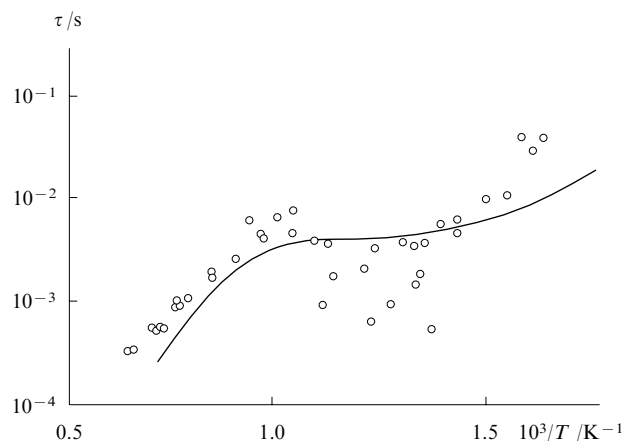
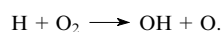


Figure 12. Comparison of calculated (line) and measured (points) delays in the ignition of a stoichiometric n-heptane–air mixture at $P_0 = 1500$ kPa.³³

autoignition delay) of the relative temperature (T/T_m) and concentrations ($[n_j]/[n_{j,m}]$) of key intermediates such as $\text{C}_7\text{H}_{15}\text{O}_2\text{H}$, H_2O_2 , OH and H, which were formed in the autoignition of a stoichiometric n-heptane–air mixture at different initial temperatures. These results show that at $T_0 = 680$ K, the multistage autoignition occurs (curves 4 in Fig. 13 a–d). In the temperature profile (Fig. 13 a), two waves are present. The first wide wave (amplitude of 150°) corresponds to the temperature rise due to the cool flame, the second shorter wave appears at the end of the induction period. Its amplitude is approximately 250° and the temperature reaches as high as ~ 1350 K. This wave corresponds to blue flame. Subsequently, the reaction transforms into hot explosion. The first temperature wave is caused by the reaction acceleration due to the stepwise increase in the concentration of OH radicals formed in the thermal decomposition of hydroperoxide $\text{C}_7\text{H}_{15}\text{O}_2\text{H}$, whereas the second wave is caused by the reaction acceleration with the next sharp increase in the OH concentration due to the thermal decomposition of more stable H_2O_2 molecules. The first slight increase in the concentration of H atoms (curve 4 in Fig. 13 e) is observed at the end of cool flame region, the second is observed in the blue flame region. After the complete decomposition of hydrogen peroxide (the end of the blue flame region), the concentrations of hydroxyl and hydrogen atoms first decrease and then sharply increase due to the branched chain reaction



Due to the vigorous progress of the reaction, the temperature begins to sharply increase and reaches its maximum, *i.e.*, the combustion temperature (is not shown in the Figure).

Figure 13 also shows the time dependences of the relative temperatures and concentrations at higher initial temperatures T_0 : 800 (curve 3), 900 (2) and 1000 K (1). These dependences provide an insight into the dynamics of variations in the temperature and concentrations of the main substances involved in the autoignition on the transition from multistage to single-stage oxidation. As the initial temperature increases to $T_0 = 900$ and 1000 K, the relative concentration of $\text{C}_7\text{H}_{15}\text{O}_2\text{H}$ (Fig. 13 c) decreases by several orders of magnitude and cannot be seen in the plot (shown by arrows), the H_2O_2 concentration decreases less sharply and the concentration of hydrogen atoms is very low during the delay at high initial

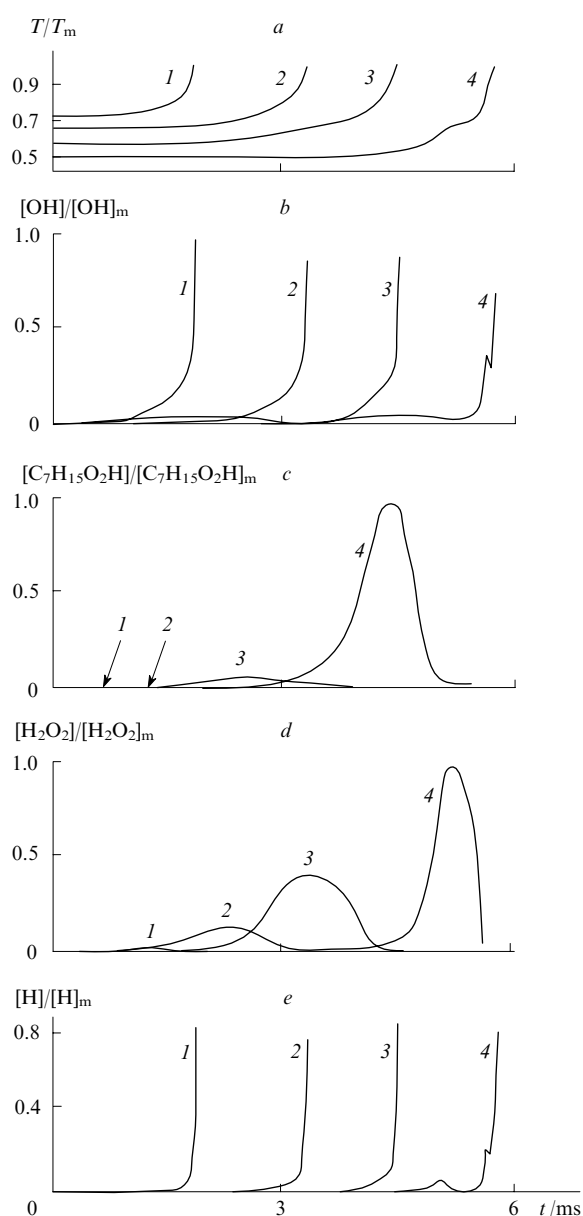


Figure 13. Dependences of relative temperatures (a) and concentrations (b–e) on time for autoignition of a stoichiometric n-heptane–air mixture at $P_0 = 1500$ kPa, $[C_7H_{16}]_0 = 1.87\%$ and different temperatures.³⁴ T_0/K : (1) 1000, (2) 900, (3) 800, (4) 680. (a) T/T_m , $T_m = 1363$ K; (b) $[OH]/[OH]_m$, $[OH]_m = 3.025 \times 10^{-4}$; (c) $[C_7H_{15}O_2H]/[C_7H_{15}O_2H]_m$, $[C_7H_{15}O_2H]_m = 8.176 \times 10^{-5}$; (d) $[H_2O_2]/[H_2O_2]_m$, $[H_2O_2]_m = 8.176 \times 10^{-5}$; (e) $[H]/[H]_m$, $[H]_m = 1.283 \times 10^{-7}$.

temperatures but quickly increases at the hot explosion to a quite considerable value for all temperatures.

Due to the fact that the temperature regions of the formation and decomposition of n-heptyl hydroperoxide are considerably lower than the regions of the formation and decomposition of hydrogen peroxide, the cool and blue flames observed at the n-heptane autoignition are well separated as in the case of acetaldehyde.

3. Propane

No blue flame was observed in the propane combustion. However, in view of similar mechanisms of oxidation and combustion of paraffin hydrocarbons, it can be assumed that propane combustion, like n-heptane combustion, may feature

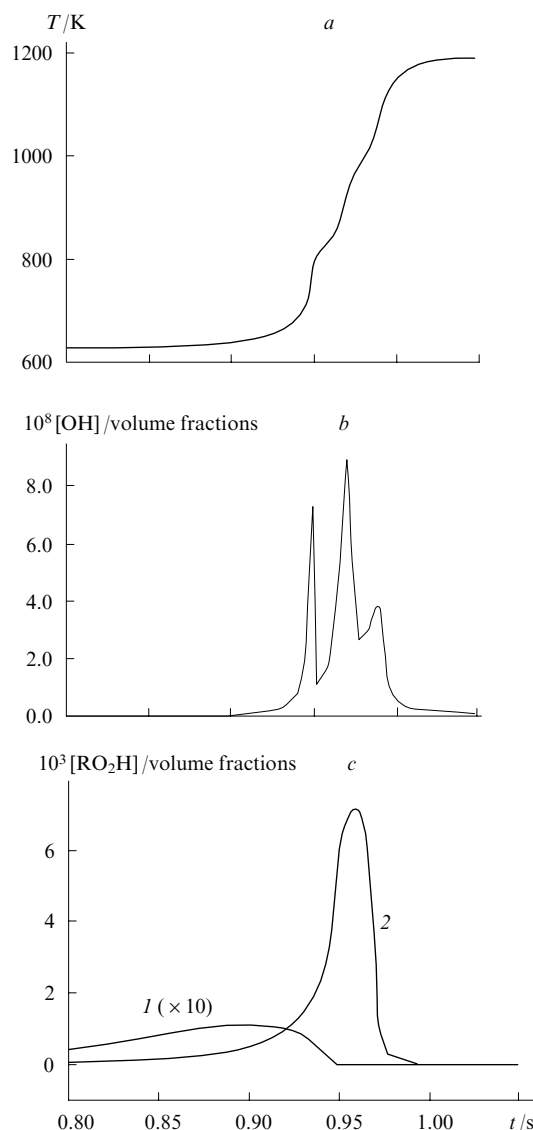


Figure 14. Calculation of autoignition of a propane–air mixture 15.5% C_3H_8 –10.5% O_2 –74% N_2 for initial conditions $T_0 = 625$ K, $P_0 = 550$ kPa.

Variations of temperature (a) and concentrations of hydroxyl (b) and hydroperoxides $C_3H_7O_2H$ (1) and H_2O_2 (2) (c).

the appearance of blue flame under appropriate conditions. As follows from the abundant experimental data on the propane oxidation and combustion that can be found in the literature (e.g., see a monograph² and references therein), its oxidation features cool flame, regions of the negative temperature coefficient (NTC) and other phenomena typical of the oxidation of higher hydrocarbons. This is why an attempt was undertaken to theoretically determine the conditions for the appearance of blue flame during low-temperature propane oxidation by modelling. The kinetic mechanism of propane oxidation and combustion was taken from Ref. 16.

Typical calculated temperature vs. time records for the autoignition of a propane–air mixture corresponds to two-stage autoignition, namely, demonstrates delays in the appearance of cool (τ_1) and hot (τ_2) flames (Fig. 14). For example, for $T_0 = 650$ K, the overall delay in the autoignition of a propane (6.5%)–air mixture was ~ 2.48 s (varied from 2.1 to 3.5 s in different experiments). Such a form of hydrocarbon autoignition is typical of low temperatures. Cool flame appears at

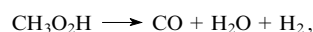
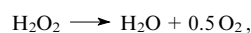
the decomposition of propyl hydroperoxide $C_3H_7O_2H$ as a result of chain branching, which leads to a sharp increase in the hydroperoxide concentration and accelerates C_3H_8 oxidation. As all accumulated hydroperoxide is consumed, the reaction decelerates and, in the next period (during the τ_2 delay) hydrogen peroxide H_2O_2 is accumulated. Its decomposition, *i.e.*, the second branching of the reaction, leads to an increase in the reaction rate and, ultimately, to hot explosion (reaction of H with O_2). Immediately before the hot explosion, a local break is observed in the smooth increase of the OH concentration, which, however, does not cause any apparent changes in the temperature growth rate. When richer propane–air mixtures are used, the irregular changes in the OH concentration manifest themselves by the appearance of the second maximum in the $[OH]$ vs. T curve. As a result, the curve demonstrates a break that corresponds to blue flame. Figures 14 *a–c* show the results of calculations of autoignition of a propane–air mixture with the 15.5% C_3H_8 –10.5% O_2 –74% N_2 ratio at $T_0 = 625$ K and $P_0 = 550$ kPa. Three inflections in the $T(t)$ curve and three maxima in the $[OH]$ vs. T curve correspond to the multistage autoignition with the appearance of cool, blue and hot flames.

4. Ethane

Until recently, no blue flame was observed in the ethane oxidation and combustion and even cool flames were discovered not long ago. The analysis of the staged mechanism of the ethane autoignition²⁹ was based on the assumption that its oxidation involves the same reactions as the oxidation of higher hydrocarbons, *i.e.*, the process includes three stages, namely, cool flame, blue flame and hot autoignition. Cool-flame phenomena may be associated with both the ethane oxidation and the oxidation of stable products and radicals that are formed in the later stages and are typical of methane oxidation.

Let us dwell on calculations²⁹ performed using a kinetic mechanism of oxidation of hydrocarbons C_1 – C_2 , which was proposed in Ref. 27 and extended by the introduction of additional reactions necessary for modelling of the cool-flame phenomena at the ethane oxidation (see Table 1). First of all, it was selectively checked whether this model adequately describes certain phenomenological characteristics of the ethane oxidation and combustion in the low and high-temperature ranges. This was necessary because the multistage ethane oxidation was never modelled earlier.

Calculations of the ethane oxidation at low temperatures and moderate pressures (*i.e.*, when the reaction time is long and the diffusion rate is sufficiently high) took into account the following effective wall reactions of the decay of active species:



In calculations, the rate constants k_w used for these reactions were the same and were close to their maximum value in the diffusion approximation. The heat-transfer coefficient was taken equal to 0.126 J litre⁻¹ s⁻¹ K⁻¹ in all cases.

The calculations of the low-temperature process were accomplished for different conditions (different mixture compositions, initial temperatures and pressures) described in the experimental study.³⁵ The experiments carried out under these conditions revealed the multiple appearance of one, two or three cool flames, where the number of cool flames increased with the diameter of the reaction vessel. On the qualitative level, the calculations²⁹ adequately described the experimentally observed cool-flame phenomena³⁵ as regards both the

time (minutes) and heating (tens of degrees). Thus at $k_w = 1$ s⁻¹, no cool flame was observed at all (this rate constant value corresponds to the highest possible diffusion rate constant under these conditions). For a rate constant $k_w = 0.35$ s⁻¹, a single cool flame was observed (manifested by an NTC). Two and three cool flames were observed for $k_w = 0.25$ s⁻¹ and $k_w = 0.12$ s⁻¹, respectively. For $k_w = 0$ (in the absence of peroxide decay on the wall), the calculations pointed to the autoignition process. The authors of experimental studies³⁵ did not observe the autoignition because they did not deal with pressures above 118 kPa.

Insofar as the calculations described rather adequately the experimental data on cool flames, the next step was the analysis and modelling of the multistage mechanism of ethane combustion under autoignition conditions. Based on the fact that $k_w = 0.353$ s⁻¹ at a pressure of 100 kPa and a temperature of 600 K, the authors calculated k_w for other pressures and temperatures. According to calculations, the autoignition begins as soon as a pressure of 150 kPa and a temperature of 560 K ($k_w = 0.23$ s⁻¹) are reached (at lower temperatures, no autoignition was observed).

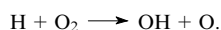
In view of the multistage autoignition mechanism, the authors of calculations considered the combustion of an ethane–oxygen equimolar mixture at $T_0 = 560$ K and $P_0 = 150$ kPa. Under these conditions, a two-stage process is observed, namely, a cool-flame flash occurs with a delay $\tau_1 = 390$ s and is accompanied by a partial energy release and a temperature rise by 104°; after a time $\tau_2 = 9$ s, hot autoignition occurs so that the overall delay turns out to be $\tau_\Sigma = \tau_1 + \tau_2 = 399$ s. As the temperature is increased from 560 to 600 K, the cool flame delay τ_1 becomes shorter and the flame intensity expressed as a temperature rise (ΔT) becomes lower. Delay τ_2 and overall delay τ_Σ increase.

Note the specific features of the autoignition kinetics in the cool-flame region. According to the analysis, during the induction period that precedes the appearance of cool flame, the accumulation of ethyl hydroperoxide $C_2H_5O_2H$ occurs and the decomposition of the latter leads to the low-temperature branching of the combustion reaction. The branching causes a temperature jump, namely, the cool-flame flash. Methyl hydroperoxide and hydrogen peroxide are also involved in the later stages of ethane combustion. In cool flame, as the temperature increases, the equilibrium in the formation of peroxide radicals $C_2H_5O_2$ shifts to the left (*i.e.*, the formation of $C_2H_5O_2$ radicals is hindered), the reaction is slowed down and the temperature stops to increase. The concentrations of CH_3O and OH radicals in the reaction mixture sharply increase 390 s after the beginning of the reaction. The increase in $[OH]$ reflects the increase in the reaction rate in cool flame. Then, the OH concentration begins to decrease, which entails a decrease in the overall reaction rate after the cool flame.

Based on the shape of kinetic curves obtained with a low resolution, one can infer on a typical two-stage mechanism of autoignition (cool flame and hot autoignition). However, at a higher time resolution, the multistage autoignition can be deduced, *i.e.*, the presence of an additional stage before the hot flame. Thus immediately before the hot autoignition, one can observe an increase in the H_2O_2 concentration and also an increase in the concentrations of C_2H_5O , CH_3O , HO_2 and HCO radicals. This violates the monotonic nature of the first derivative of $T(t)$. At the same time, a new considerable increase in the OH concentration is observed, which points to the acceleration of the ethane oxidation. Modelling makes it possible to find the factor responsible for this acceleration. Thus, if in the middle of the considered time interval, the rate constants of each branching reaction, namely, the rate constants for the decomposition of $C_2H_5O_2H$, CH_3O_2H and H_2O_2 are in turn put to zero, this will not affect the increase in the OH concentration for the case of alkyl peroxides, whereas for

H_2O_2 , this will lead to a decrease in the OH concentration and, hence, to the increase in the reaction rate and the temperature. Hence, one can unambiguously conclude that the reaction branching due to the H_2O_2 decomposition is the main reason for the reaction acceleration. This very increase in the ethane oxidation rate prior to hot flame is defined as the blue flame and allows one to assume the multistage mechanism of the ethane autoignition.

In hot flame (the third stage of autoignition), the chief role in the reaction branching is played by the process



Within the framework of a concept of multistage autoignition of paraffin hydrocarbons, a kinetic scheme of ethane combustion was proposed,²⁹ which contains the following stages: (1) cool-flame stage (reaction branching occurs due to the decomposition of hydroperoxides $\text{C}_2\text{H}_5\text{O}_2\text{H}$, $\text{CH}_3\text{O}_2\text{H}$ and also of a part of H_2O_2), (2) blue-flame stage, which precedes hot autoignition (reaction branching due to the decomposition of hydrogen peroxide) and (3) hot-flame stage (reaction branching due to the reaction of H radicals with oxygen).

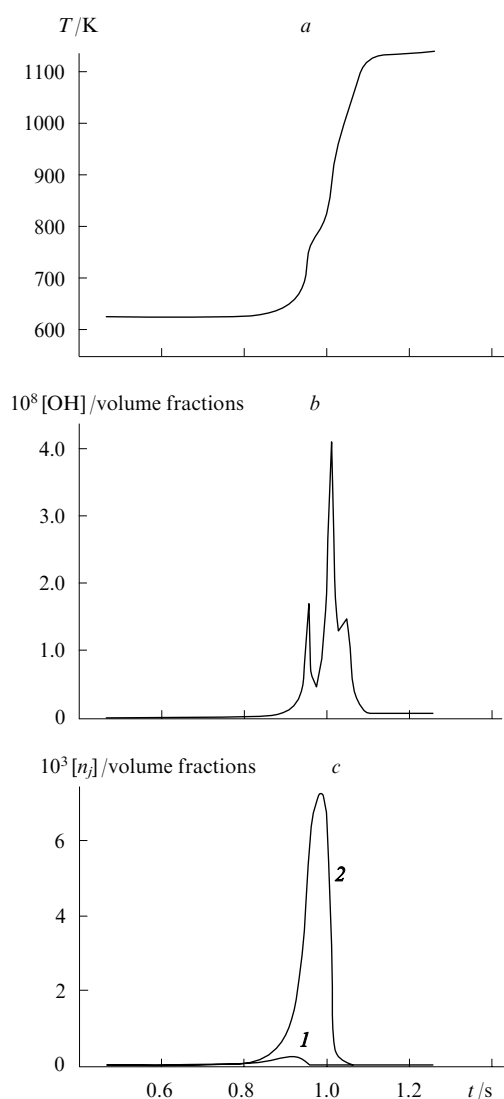


Figure 15. Calculated time dependences of temperature (*a*) and concentrations [OH] (*b*), $[\text{C}_2\text{H}_5\text{O}_2\text{H}]$ (*c*, curve 1) and of H_2O_2 (*c*, curve 2) for autoignition of an ethane–air mixture 16.5% C_2H_6 –9.5% O_2 –74% N_2 for initial conditions $T_0 = 625$ K and $P_0 = 550$ kPa.

In mixtures richer in ethane, the break of the smooth increase in the concentration [OH] manifests itself by the appearance of the second maximum in the [OH] vs. t curves and a bend in the T vs. t curve, which correspond to blue flame (later calculations¹⁶). As the example, Fig. 15 *a–c* shows the results of calculations of the autoignition of an ethane–air mixture with the composition 16.5% C_2H_6 –9.5% O_2 –74% N_2 for $T_0 = 625$ K at $P_0 = 550$ kPa. Here, as for the propane oxidation, three bends are present in the temperature curve and three maxima appear in the [OH] vs. t curve, which correspond to the multistage autoignition with generation of cool, blue and hot flames.

In the case of ethane, ethyl hydroperoxide plays the chief role in the appearance of cool flames. The closeness of the temperature interval of its decomposition to the temperature interval of hydrogen peroxide decomposition complicates the separation of the cool-flame and blue-flame stages.

5. Methane

The first mention³⁶ of the multistage mechanism of low-temperature oxidation of methane dates back to 1956. In this study, two stages in this process, namely, cool-flame oxidation and autoignition, were observed experimentally.

The first attempt to model the methane autoignition within the framework of a relatively simple kinetic scheme was undertaken in 1982 (Ref. 37) and, although the kinetic scheme used in calculations was developed for modelling of the combustion processes and was supplemented by merely few reactions typical of the low-temperature range of methane oxidation, the results obtained demonstrated the possibility of describing the staged nature of the methane oxidation.

The later calculations employed a kinetic scheme specially developed for the description of low-temperature oxidation of rich methane mixtures.³⁸ Figure 16 shows the results of such calculations.³⁹ As is seen, at the initial temperatures $T_0 < 710$ K, the staged nature of the reaction was not manifested (curve 1). For $T_0 > 758$ K (curves 5–7), ignition occurred (arrows at the ends of curves point to the further increase in the temperature). In the temperature range $T_0 = 728$ –753 K, flashes with incomplete heat release were observed which were followed by reaction inhibition accompanied by a temperature decrease due to the cooling of the reaction mixture by the reactor walls. As a whole, the calculated data corresponded to experimental results described,³⁶ which made it possible to use this kinetic scheme in predicting the behaviour of this reaction under high-pressure conditions

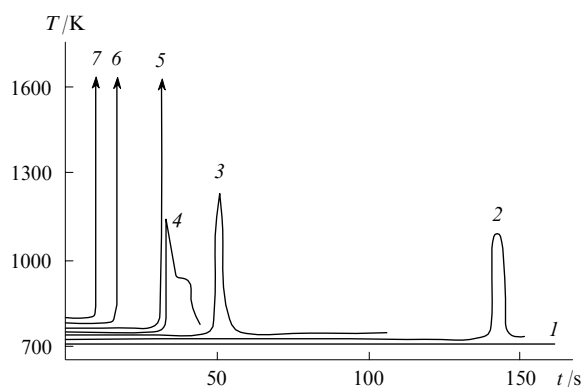


Figure 16. Time dependences of temperature during the oxidation of methane–oxygen mixtures for different initial temperatures.³⁹ Initial conditions: $[\text{CH}_4]_0 = 67\%$, $[\text{O}_2]_0 = 33\%$, $P_0 = 92$ kPa, $\kappa S/V = 6.61$ J cm^{-3} s^{-1} K^{-1} ; T_0/K : (1) 710, (2) 728, (3) 748, (4) 753, (5) 758, (6) 768 and (7) 788.

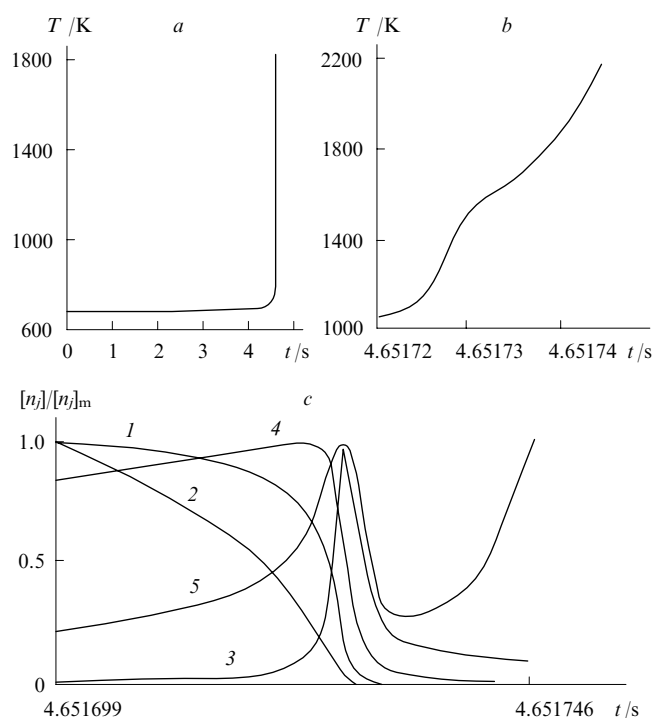


Figure 17. Dependences of (a, b) temperature and (c) concentrations on the reaction time on time scales of (a) seconds and (b, c) microseconds during the oxidation of a methane–oxygen mixture.³⁹

Initial conditions: $[\text{CH}_4]_0 = 67\%$, $[\text{O}_2]_0 = 33\%$, $T_0 = 710$ K, $P_0 = 7000$ kPa.

(c) (1) $[\text{H}_2\text{O}_2]/[\text{H}_2\text{O}_2]_m$, $[\text{H}_2\text{O}_2]_m = 2.279 \times 10^{-6}$; (2) $[\text{CH}_3\text{O}_2\text{H}]/[\text{CH}_3\text{O}_2\text{H}]_m$, $[\text{CH}_3\text{O}_2\text{H}]_m = 1.412 \times 10^{-8}$; (3) $[\text{HO}_2]/[\text{HO}_2]_m$, $[\text{HO}_2]_m = 1.619 \times 10^{-6}$; (4) $[\text{CH}_3\text{O}_2]/[\text{CH}_3\text{O}_2]_m$, $[\text{CH}_3\text{O}_2]_m = 2.156 \times 10^{-7}$; (5) $[\text{H}]/[\text{H}]_m$, $[\text{H}]_m = 1.420 \times 10^{-8}$.

for which no experimental data could be obtained in static setups.

Calculations were carried out for the mixture 67% CH_4 –33% O_2 at the initial temperature of 710 K and different initial pressures (from 180 to 10 000 kPa). It was found that as the pressure increases, the transition from oxidation to autoignition occurs and the latter is reached in shorter times. Even active heat transfer from the gas to the reactor walls (within reasonable heat transfer coefficients) fails to stop the ignition and reverse the temperature increase, although the heat transfer increases the time the oxidation reaction develops to the autoignition. Figure 17a shows the

typical temperature dependence for the methane oxidation on a time scale of seconds.³⁹ With this resolution, the curve shows no indications of the multistage mechanism. Based on the shape of this curve, the methane oxidation can be assigned to conventional single-stage autoignition processes. However, curve $T(t)$ recorded at a rapid temperature-*vs.*-time scanning (on a microsecond time scale, Fig. 17b) has a bend, which suggests that the temperature rise to $T = 1400$ K is followed by the reaction retardation with the subsequent hot flash in approximately 15 μs , *i.e.*, the multistage nature of the reaction is evident. In this case, the duration of the first combustion stage was ~ 4.6 s, and the duration of the second stage was 15 μs (it is very difficult to experimentally observe two stages within such times). The staged nature is evident most clearly in the concentration profiles of hydroperoxides $\text{CH}_3\text{O}_2\text{H}$ and H_2O_2 , and also of radicals HO_2 , CH_3O_2 and H shown on a microsecond scale (see Fig. 17c).

A similar situation was also observed at 750 K and higher, at which the autoignition process that looks as a single-stage process occurs. Calculations of the oxidation of methane–air mixtures were also carried out for the lower oxygen contents, a pressure $P_0 = 10\,000$ kPa and temperatures $T_0 = 683$ –750 K. It was shown that with a decrease in the oxygen content, the indications of the staged mechanism become less pronounced and totally disappear at $[\text{O}_2]_0 = 5\%$.

In the calculations of oxidation processes under high-pressure conditions, the limiting values of reaction rate constants for the infinitely high pressure were taken (the corresponding data can be found in Table 2).

The detection of blue flames in experiments carried out in ICE near the autoignition limits of lean methane–air mixtures served as evidence for the multistage mechanism of hydrocarbon autoignition.⁴⁰

An attempt⁴¹ was made to model blue flames experimentally observed in ICE⁴⁰ by using a kinetic scheme of the process and a computer code that takes into account the piston motion. The analysis of methane oxidation in ICE made it possible to explain the illusory contradiction between the experimental data obtained in ICE⁴⁰ and in a static setup.⁴² Methane oxidation was frozen on the piston back stroke, which makes it possible to establish the initial conditions corresponding to the cessation of the relatively slow initial reaction. In a static bomb, such conditions favourable for the reaction suppression are absent.

For calculations, the same conditions as in the ICE experiments⁴³ were taken (the compression ratio $\varepsilon = 14.7$ for a speed $n = 1000$ rpm) (the calculations were carried out according to a kinetic scheme that can be found in Ref. 26 and Table 1). According to calculations, as the compression temperature changes, in the range of low methane concentration, there is a

Table 2. Kinetic parameters of high-pressure oxidation of C_1 – C_2 hydrocarbons.

Reaction number ^a	Reactions	$H/\text{kJ mol}^{-1}$	Forward reaction			Reverse reaction		
			A^b	n	$E/\text{kJ mol}^{-1}$	A^b	n	$E/\text{kJ mol}^{-1}$
7	$\text{OH} + \text{H} \rightleftharpoons \text{H}_2\text{O}$	494.04	6.8×10^{10}	0.1	0.00	1.6×10^{15}	–0.9	502.42
10	$\text{H} + \text{O}_2 \rightleftharpoons \text{HO}_2$	196.78	1.2×10^9	0.6	0.00	1.6×10^{12}	–0.4	204.32
17	$\text{OH} + \text{OH} \rightleftharpoons \text{H}_2\text{O}_2$	209.34	3.4×10^7	1.0	0.00	1.0×10^{16}	0.0	209.34
24	$\text{CO} + \text{O} \rightleftharpoons \text{CO}_2$	531.72	1.0×10^4	1.0	10.47	9.0×10^{12}	0.0	544.28
34	$\text{HCO} + \text{H} \rightleftharpoons \text{HCHO}$	305.64	7.1×10^5	1.6	62.80	5.9×10^{13}	0.6	376.81
42	$\text{H} + \text{CH}_3 \rightleftharpoons \text{CH}_4$	422.87	8.4×10^7	0.0	0.00	1.8×10^{16}	0.0	439.61
71	$\text{H} + \text{HCHO} \rightleftharpoons \text{CH}_3\text{O}$	92.11	2.8×10^7	1.0	10.05	3.0×10^{14}	0.0	108.86
76	$\text{C}_2\text{H} + \text{H} \rightleftharpoons \text{C}_2\text{H}_2$	523.35	1.4×10^5	1.0	–54.43	8.5×10^{12}	0.0	447.99
81	$\text{H} + \text{C}_2\text{H}_2 \rightleftharpoons \text{C}_2\text{H}_3$	167.47	5.5×10^9	0.0	10.05	2.6×10^{16}	–1.0	194.27

^a The reaction number corresponds to that in Table 1. ^b The pre-exponential factor A is expressed in s^{-1} for unimolecular reactions, in $\text{litre mol}^{-1} \text{s}^{-1}$ for bimolecular reactions and in $\text{litre}^2 \text{mol}^{-2} \text{s}^{-1}$ for trimolecular reactions.

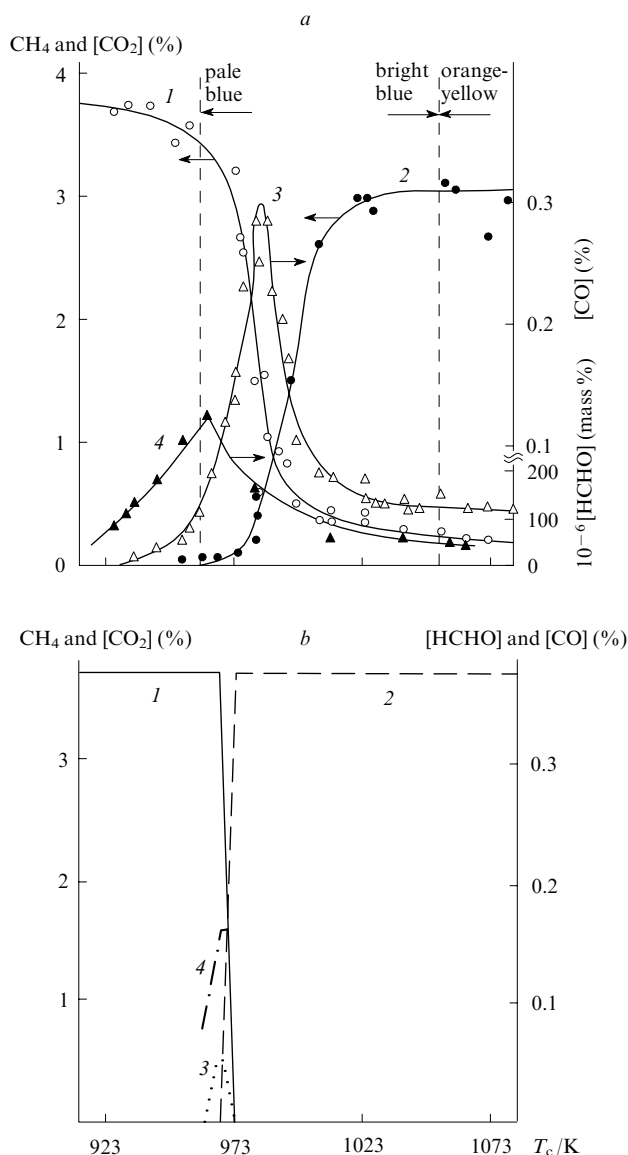


Figure 18. Experimental (a)⁴³ and calculated (b)⁴¹ dependences of relative concentrations of CH₄ (curve 1), CO₂ (2), CO (3) and HCHO (4) on the final compression temperature T_c during the oxidation of a methane–air mixture.

Initial conditions: $[\text{CH}_4]_0 = 3.7\%$, $\varepsilon = 14.7$, $n = 1000$ rpm.

transition from the reaction absence to the complete combustion through the region of incomplete heat release typical of cool and blue flames. In Fig. 18, the dashed lines mark the transition region of the methane incomplete oxidation and combustion, which was experimentally obtained for $[\text{CH}_4]_0 = 3.7\%$. This region extends from 963 to 1053 K, *i.e.*, approximately for 90°. This region revealed experimentally in Ref. 43 was assigned to blue flames. In the calculations (see Fig. 18b) with the same methane concentrations, the blue flame region was merely 1°. As the $[\text{CH}_4]_0$ decreased, the blue flame region extended to 10°. Thus Fig. 19 shows the changes in pressure (curve 1), temperature (curve 2) and concentrations of CH₄, OH, HCHO, CO and CO₂ (curves 3–7) in this transition region. It is evident that methane is partially oxidised to form a certain amount of CO and a very small amount of CO₂. The heat released in the process does not considerably increase the pressure or the temperature.

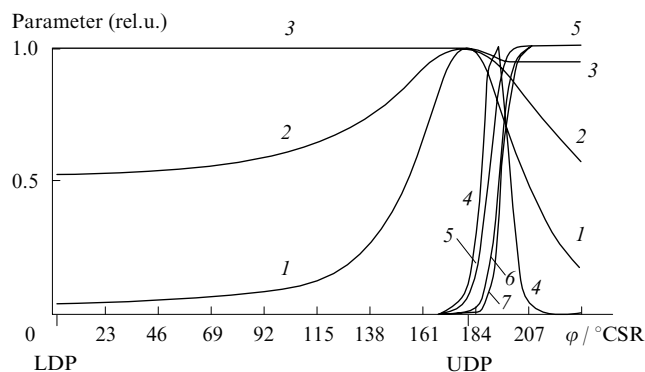
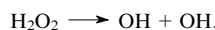


Figure 19. Diagram of autoignition of a methane–air mixture containing 3.7% CH₄, for $T_c = 968$ K, $\varepsilon = 14.7$, $n = 1000$ rpm.

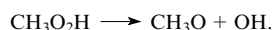
Here, LDP and UDP are the lower (0°) and upper (180°) dead points, CSR are crankshaft rotations.

(1) P/P_m , $P_m = 3510$ kPa; (2) T/T_m , $T_m = 968$ K; (3) $[\text{CH}_4]/[\text{CH}_4]_m$, $[\text{CH}_4]_m = 3.7\%$; (4) $[\text{OH}]/[\text{OH}]_m$, $[\text{OH}]_m = 6.3 \times 10^{-4}\%$; (5) $[\text{HCHO}]/[\text{HCHO}]_m$, $[\text{HCHO}]_m = 0.16\%$; (6) $[\text{CO}]/[\text{CO}]_m$, $[\text{CO}]_m = 5.5 \times 10^{-2}\%$; (7) $[\text{CO}_2]/[\text{CO}_2]_m$, $[\text{CO}_2]_m = 2.5 \times 10^{-4}\%$.

The reason for the staged mechanism of methane oxidation and the incomplete heat release in the transition region is sequence of poorly separated main branching processes that arise in the decomposition of methyl hydroperoxide and hydrogen peroxide. Thus the analysis of the oxidation kinetics of a lean methane–air mixture under the conditions described in Ref. 43 showed that the branching of active sites takes place mainly due to the reaction



In this case, the OH concentration first increases and then, after the consumption of all accumulated H₂O₂, starts to decrease. This is why only a part of methane is consumed in the reaction. A hypothetical mathematical experiment in which the rate constant for the H₂O₂ decomposition is set equal to zero in the very beginning shows that virtually no methane can be oxidised under ICE conditions.⁴³ Methyl hydroperoxide CH₃O₂H is the main branching product in the cool-flame oxidation of methane; its decomposition yields hydroxyl



Under the chosen conditions, due to the relatively high initial temperature, only a small amount of CH₃O₂H is formed. Nonetheless, if we set the rate constant for the CH₃O₂H decomposition equal to zero, the methane oxidation is slowed and the yield of products becomes several times lower. Thus, non-separated mixed cool and blue flames were observed in the methane oxidation under these conditions.

All studies devoted to the stepwise mechanism and the pre-flame reactions in the methane oxidation described either cool or blue flames; however, no publications reported on the separate observation of these stages in one experiment. Apparently, it can be concluded that these flames exist only as a united ‘cool-blue flame’ that features the peculiarities of both stages.

Figure 20 shows calculated time dependences of the relative temperature (a) and relative concentrations of hydroxyl (b) and hydroperoxides (c) in the oxidation of rich methane–oxygen mixtures. One can see the regions of the origination of the pre-flame reaction (from 1 to 2.5–3 s) and hot autoignition (at ~7.5 s). As seen, the ranges where the temperature rises and the OH concentration increases are situated in the regions

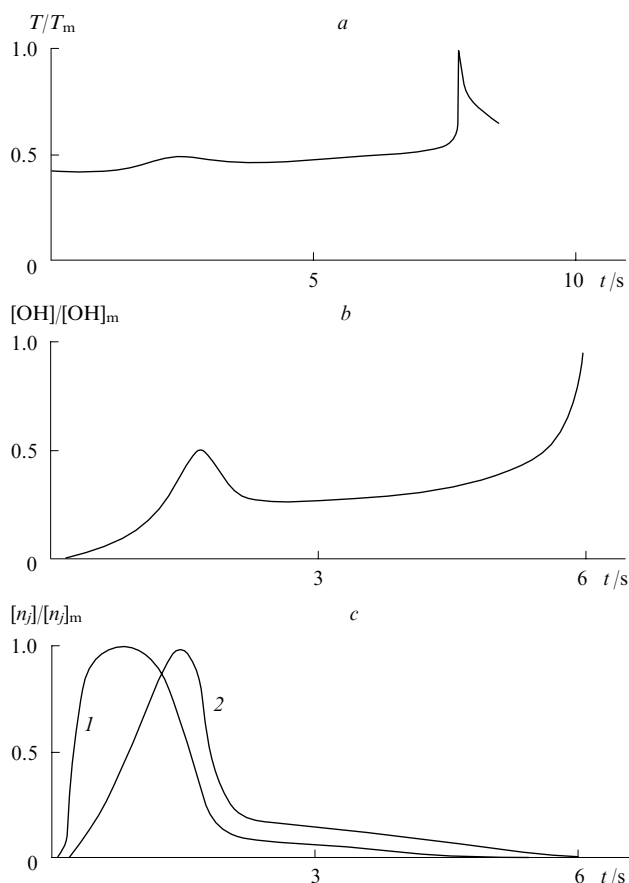


Figure 20. Time dependences of relative temperature T/T_m (a) and relative concentrations of OH (b), $\text{CH}_3\text{O}_2\text{H}$ (c, curve 1) and H_2O_2 (c, curve 2) in the oxidation of a methane–oxygen mixture. Initial conditions: $[\text{CH}_4]_0 = 67\%$, $[\text{O}_2]_0 = 33\%$, $P_0 = 122$ kPa, $\kappa S/V = 6.61$ J cm^{-3} s^{-1} K^{-1} , $T_m = 1849$ K, $[\text{OH}]_m = 5.43 \times 10^{-9}$, $[\text{CH}_3\text{O}_2\text{H}]_m = 4.19 \times 10^{-5}$, $[\text{H}_2\text{O}_2]_m = 8.60 \times 10^{-2}$.

corresponding to the decomposition of $\text{CH}_3\text{O}_2\text{H}$ (1.3 s) and H_2O_2 (2.6–3 s). Modelling of a process during which the rate constants for the $\text{CH}_3\text{O}_2\text{H}$ and H_2O_2 decomposition decreased one after another has led to a dramatically different pattern of the overall autoignition process, which reflects the effects of both branching reactions on the pre-flame processes. This substantiates a conclusion that the separation of cool and blue flames in the methane oxidation reaction is a difficult and even impossible task and these processes occur simultaneously (with a very short time lag).

IV. Conclusion

Experimental and calculated data obtained based on the detailed kinetic mechanisms of the oxidation of hydrocarbons and their derivatives demonstrate that blue flame arises due to the decomposition of hydrogen peroxide formed in the hydrocarbon oxidation. This is typical of all reactions of oxidation and combustion of hydrocarbons and their derivatives. Blue flame was observed in the gas-phase oxidation and combustion of methane, ethane, n-heptane, isooctane, benzene, acetaldehyde and diethyl ether. Blue flames were clearly observed in the oxidation of acetaldehyde and n-heptane and less clearly in the ethane oxidation. In the methane oxidation, mixed 'cool-blue flame' was observed.

The division of the oxidation process at autoignition into stages is not always possible. Depending on the fuel type, the mixture composition, temperature and pressure, the contribu-

tions of individual stages into the overall oxidation rate can change. These contributions may overlap, which makes impossible their separation. However, the essence of the stepwise mechanism, *i.e.*, the involvement of different reaction groups that make their own contributions to the branching and oxidation, remains unchanged. For example, in the ethane oxidation, the stages corresponding to individual contributions of the $\text{C}_2\text{H}_5\text{O}_2\text{H}$ and $\text{CH}_3\text{O}_2\text{H}$ decomposition reactions could not be separated probably due to their very close kinetic characteristics. In connection with this, it is interesting to analyse the oxidation of heavy paraffin hydrocarbons with the larger number of carbon atoms in molecules for which the kinetic characteristics of the decomposition of the main ($\text{C}_n\text{H}_{2n+1}\text{O}_2\text{H}$) and secondary hydroperoxides are not so similar. At present, when the scientists have at their disposal such fast-response analytical instruments that allow them to study the reactions of hydrocarbon oxidation, the implementation of such a study would be extremely desirable.

References

1. H Perkin *J. Chem. Soc.* **41** 363 (1882)
2. V Ya Shtern *Mekhanizm Okisleniya Uglevodorodov v Gazovoi Faze* (Mechanism of Gas-Phase Oxidation of Hydrocarbons) (Moscow: Izd. Akad. Nauk SSSR, 1960)
3. A S Sokolik *Samovosplamnenie, Plamya i Detonatsiya v Gazakh* (Autoignition, Flame and Detonation of Gases) (Moscow: Izd. Akad. Nauk SSSR, 1960)
4. B Lewis, G Elbe *Combustion, Flames and Explosions of Gases* (Orlando: Academic Press, 1987)
5. M B Neiman *Usp. Khim.* **7** 341 (1938)
6. J Bardwell, C N Hinshelwood *Proc. R. Soc. London, Ser. A* **205** 375 (1951)
7. N M Chirkov, S G Entelis *Kinetika Tsepnykh Reaktsii Okisleniya* (Kinetics of Chain Oxidation Reactions) (Moscow: Izd. Akad. Nauk SSSR, 1950) p. 118
8. J E C Topps, D T A Townend *Trans. Faraday Soc.* **42** 345 (1946)
9. Y Ohta, H Takahashi *Progress in Astronautics and Aeronautics* Vol. 88 (Reston, VA: AIAA, 1983) p. 38
10. Y Ohta, H Takahashi *Progress in Astronautics and Aeronautics* Vol. 95 (Reston, VA: AIAA, 1984) p. 236
11. L V Karmilova, N S Enikolopyan, A B Nalbandyan, N N Semenov *Zh. Fiz. Khim.* **34** 1177 (1960)^a
12. B Natarajan, F V Bracco *Combust. Flame* **57** 179 (1984)
13. C T Bowman *Combust. Sci. Technol.* **2** 161 (1970)
14. S Refael, E Sher *Combust. Flame* **78** 326 (1989)
15. J S Hoffman, W Lee, T A Litzinger, D A Santavicca, W J Pitz *Combust. Sci. Technol.* **77** 95 (1991)
16. V Ya Basevich, V I Vedenev, S M Frolov, L B Romanovich *Khim. Fiz.* **25** (11) 87 (2006)^b
17. W J Pitz, C K Westbrook *Combust. Flame* **63** 113 (1986)
18. S Kojima *Combust. Flame* **99** 87 (1994)
19. C K Westbrook *AIAA J.* **24** 2002 (1986)
20. A Chakir, M Belumam, J C Boettner, M Cathonnet *Combust. Sci. Technol.* **77** 239 (1991)
21. M Bui-Pham, K Seshadri *Combust. Sci. Technol.* **79** 293 (1991)
22. E Ranzi, T Faravelli, P Gaffuri, A Sogaro *Combust. Flame* **102** 179 (1995)
23. H J Curran, P Gaffuri, W J Pitz, C K Westbrook *Combust. Flame* **114** 149 (1998)
24. H J Curran, P Gaffuri, W J Pitz, C K Westbrook *Combust. Flame* **129** 253 (2002)
25. L L Skrumeda, J Ross *J. Phys. Chem.* **99** 12835 (1995)
26. V Ya Basevich, V I Vedenev, L B Romanovich *Khim. Fiz.* **22** (7) 60 (2003)^b
27. V Ya Basevich *Handbook of Heat and Mass Transfer* Vol. 4 (Ed. N Chermisinoff) (Houston: Gulf, 1990) p. 769
28. V Ya Basevich, V I Vedenev, V S Arutyunov *Khim. Fiz.* **18** (6) 40 (1999)^b
29. V Ya Basevich, V I Vedenev, V S Arutyunov *Khim. Fiz.* **17** (5) 73 (1998)^b

30. A A Belyaev, V S Posvyanskii *Gosudarstvennyi Fond Algoritmov i Programm SSSR. Algoritmy i Programmy. Informatsionnyi Byulleten'* (Consolidated Fund of Algorithms and Programmes of the USSR. Algorithms and Programmes. Information Bulletin) (Moscow: VNTITsENTR, 1985) No. 3, p. 35
31. V N Kondrat'ev, E E Nikitin *Kinetika i Mekhanizm Gazofaznykh Reaktsii* (Kinetics and Mechanism of Gas Reactions) (Moscow: Nauka, 1974)
32. V Ya Basevich, V I Vedeneev, V S Arutyunov *Khim. Fiz.* **19** (11) 94 (2000)^b
33. V Ya Basevich, A A Belyaev, V Brandstetter, M G Neigauz, R Taschl, S M Frolov *Fiz. Goren. Vzryva* **30** (6) 15 (1994)^c
34. V Ya Basevich, V I Vedeneev, S M Frolov, L B Romanovich *Khim. Fiz.* **24** (2) 77 (2005)^b
35. J H Knox, R G W Norrish *Trans. Faraday Soc.* **50** 928 (1954)
36. M Vanpee *C. R. Acad. Sci.* **243** 804 (1956)
37. V Ya Basevich, S M Kogarko *Izv. Akad. Nauk SSSR, Ser. Khim.* 2658 (1982)^d
38. V I Vedeneev, M Ya Gol'denberg, N I Gorban', M A Teitel'boim *Kinet. Katal.* **29** 7 (1988)^e
39. V Ya Basevich, V I Vedeneev, V S Arutyunov *Khim. Fiz.* **13** (8–9) 157 (1994)^b
40. F C Egerton, N P W Moor, W T Lyn *Nature (London)* **167** 191 (1951)
41. V Ya Basevich, V I Vedeneev *Khim. Fiz.* **20** (5) 119 (2001)^b
42. J D Broatch, A C Egerton *Fuel* **31** 494 (1952)
43. A G Gaydon, N P W Moore, J R Simonson *Proc. R. Soc. London, Ser. A* **230** 1 (1955)

^a — *Russ. J. Phys. Chem. (Engl. Transl.)*

^b — *Chem. Phys. Rep. (Engl. Transl.)*

^c — *Comb. Explos. Shock Waves (Engl. Transl.)*

^d — *Russ. Chem. Bull., Int. Ed. (Engl. Transl.)*

^e — *Kinet. Catal. (Engl. Transl.)*